UNIVERSITY OF TROMSØ UIT

FACULTY OF SCIENCE AND TECHNOLOGY
DEPARTMENT OF PHYSICS AND TECHNOLOGY

Temperature sensitivity of waveguide Mach-Zehnder interferometer

Viktor Sokolov

FYS-3900 Master's Thesis in Physics

May 2013

Abstract

In the field of integrated optics a large progress has been done since its introduction more than fifty years ago. The level of integration of integrated optic components has increased gradually over the years. Primarily, this is due to the continuous development of three factors: optical waveguides, lasers and advances in fabrication technologies. The scope of integrated optical devices varies. They are used in optical communication systems, signal processing and optical sensors. Integrated optical sensors can offer several advantages over conventional electronic devices. In general, optical devices are made with dielectric materials which are chemically inert. This leads to electrical and chemical passivity, which makes them suitable for applications in hostile environments or if there is a risk of explosion. Given the sizes and nature of optical waveguides, small and light-weight devices can be made.

This thesis is part of a project that aims to develop a sensor for the detection of methane in the air and in water based on a waveguide Mach-Zehnder interferometer (MZI). The main application of this sensor is monitoring the environment and the ability to detect a leakage of methane. The development of a sensor includes analysis of operational conditions. In this project one of the greatest concerns is temperature. The temperature difference can reach several tens of degrees in the air, and several degrees in the sea. This thesis will focus on the temperature effect on the sensor output, rather than on the measurement of methane. The aim is to study sensitivity of the devices in order to reduce the temperature dependence during further measurements of methane concentration.

The results of experimental work show the conformity with theoretical analysis and demonstrate that there is no significant dependence between the temperature change and the output power from the straight waveguide, as well as from the balanced Mach-Zehnder interferometer. Observed variation in the output power from unbalanced interferometer is 0.9 dB for 10°C change in temperature, when the estimated variation is 1.1 dB.

Contents

List of figures

Acknowledgements

I would like to express my deepest appreciation to all those who provided me the possibility to complete this project. I am heartily thankful to my supervisor, professor Olav Gaute Hellesø, whose contribution helped me to coordinate and write this thesis.

I would also like to acknowledge with much appreciation all members of our optics group: Susan, Balpreet, Petter and Jean-Claude for a very enjoyable time during our optics meetings. Special thanks goes to my friend Firehun, with whom we spent many days in the lab, conducting experiments, and a little less time playing table tennis in the basement of our building.

I am taking this opportunity to express my gratitude to Norwegian State Educational Loan Fund - Lånekassen for scholarship grant during my study, and to convey thanks to the Department of Physics and Technology for a chance to be enrolled as an international student at the University of Tromsø.

Finally, I would like to thank my family and friends. They always support and encourage me with their best wishes.

Thanks for helping, everyone.

Nomenclature

MZI	Mach-Zehnder interferometer
I	Intensity
φ	Phase
λ	Wavelength
n_{eff}	Effective refractive index
T	Temperature
α_L	Linear expansion coefficient
α_n	Thermo-optic coefficient
RIU	Refractive index unit
PCB	Printed circuit board
LPCVD	Low-pressure chemical vapor deposition
PDMS	Polydimethylsiloxane
GDS	Graphic data system
CIF	Caltech intermediate form
R	Curvature radius
ω	Angular frequency
k_z	Propagation constant
$\frac{d\theta}{dt}$	Angular velocity
v_{tan}	Tangential velocity
x	Distance from the waveguide axis
n	Refractive index
W	Rib width
h	Rib depth
H	Core height
PDA	Photocurrent measurement module

TEC	Temperature control module
BNC	Bayonet-Neill connector
VI	Virtual Instrument
P_{out}	Output power
P_{ref}	Reference power
P_{rel}	Relative power

Chapter 1

Introduction to optical sensing

1.1 Motivation and objective

This thesis is part of a project aimed at the development of sensors for the detection of methane and changes in its concentration in the air and in water. Methane is the primary component of natural gas, and these sensors are important for monitoring the environment, measuring explosive gasses and during oil and gas exploration. They should be able to detect methane as a climate gas in atmosphere as well as its leaks. The effective gas leak detection devices have to be utilized in certain situations where there is a risk that methane can cause explosion or asphyxiation.

The development of the sensors is based on optical waveguides and integrated optics. The reasons for using integrated optical devices are a small size and high sensitivity. The principle of the sensor is based on chemical and physical properties of the components. The molecule of methane is highly symmetrical, uncharged and capable of interacting with its environment only via weak van der Waals forces. Since this, it is extremely difficult to bind. However, a material called cryptophane is found to be highly effective at binding methane [1]. Cryptophane is deposited on the top of a sensing waveguide, which in our project is a branch of a Mach-Zehnder interferometer.

Interacting with methane, cryptophane changes its refractive index. In turn, the evanescent field of the waveguide is affected by the variation of cryptophane refractive index and causes phase shift because only one arm of the interferometer is influenced by contact with cryptophane. Phase shift leads to difference in the power output, which is measured and analyzed during the experiments.

The development of any environmental sensor includes analysis of operational conditions. Regarding this project, one of the greatest concerns is temperature. The temperature difference can reach several tens of degrees for a sensor in air, and several degrees in the sea.

This thesis will focus on the temperature effect on the sensor output, rather than on the measurement of methane. The aim is to study sensitivity of the waveguides in order to reduce the temperature dependence during further measurements of methane concentration.

1.2 Introduction to integrated optical devices

This sensor is a part of integrated optical devices, which use light to measure a change in material properties, particularly variation in refractive index, due to external factors. The scope of integrated optical devices, in particular integrated optical sensors, has been gradually developed since their introduction [2]. It is now more than forty years since the name “integrated optics” emerged [3].

The first theoretical study of wave propagation in dielectric waveguides appeared in 1910 [4]. The discovery of the laser in the 1960s has had a tremendous impact on the development of optical devices. It was recognized as the carrier source which was so essential for light transmission techniques. During this period of the early 1960s, research in dielectric waveguides was mainly theoretical [5] [6]. After the first proposal in 1966, the group of scientists at Corning Glass Works achieved a goal of fabricating a single mode fiber with attenuation less than 20 dB/km [7]. It was enough to start the replacement of the wires by optical fibers in the communication infrastructure.

Through the fiber optic telecommunication revolution, fiber optic sensor technology has experienced a strong growth [8] [9] [10]. Along with the availability of low-loss optical fibers, there was an idea of compact optical systems. By that time the field of thin-film technology was well developed and many researchers were interested in applying the same thin-film technology in optical devices, since it was found that a thin layer of dielectric film can be a perfect waveguide if it has a refractive index larger than the refractive index of the surrounding media [11].

With small components it could be possible to combine several devices on a common substrate to form more advanced and complicated integrated optical circuits, where the problems of alignment and mechanical drift would be eliminated [12].

Among the studies that were conducted in this area, can be called the work of R.G. Heideman [13], F. Rehouma [14] and many others. Two main groups which all the optical sensors can be split into are: sensors based on intensity change and those which use a perturbation of the evanescent field of a guided mode. The evanescent wave located in the superstrate directly interacts with the sensitive medium. Sensors using evanescent field are very sensitive due to interaction length which can be relatively long. One of the most studied and developed structures in this group is a Mach-Zehnder interferometer (MZI). In the interferometer variation of the refractive index is transformed into a phase change [14].

Talking about optical devices, it is important to define terms such as “optical waveguide” and “integrated optics”. Optical waveguides are the basic elements for confinement and transmission of light. The principle of optical confinement using high dielectric materials is based upon the phenomenon of total internal reflection. The distance of transmission may vary, ranging from tens or hundreds of μm in integrated optics to hundreds or thousands of km in fiber-optic transmission. A dielectric waveguide typically consists typically of a core layer sandwiched between two layers which form the cladding. It is necessary that the core refractive index is greater than the refractive index of the cladding for the waveguide to have guidance properties. Optical waveguide can be compared to a metallic strip in an electrical integrated circuit. Rather than connecting electrical components, the optical waveguide is the fundamental element that interconnects the various devices of an optical integrated circuit. The power carrier in the waveguide is an optical wave that

travels through it in distinct optical modes. A mode is a spatial distribution of optical energy in one or more dimensions that remains constant in time and space [15].

The concept of "integrated optics" was proposed in 1969 by S.E. Miller [3]. The original idea of integrated optics came from the technology of electronic integrated circuits, which has shown rapid development, for instance emergence of microprocessors, computer memory chips etc. Integrated optics involves the use of photons instead of electrons, creating integrated optical circuits (IOC). The principal motivation for integrated optics is the ability to combine individual waveguide devices into a functional optical system incorporated onto a small substrate. This system of embedded components could include lasers, lenses, polarizers, interferometers and so forth.

Unfortunately, the progress of microelectronics technology went far further than integrated optics because of the complexity of the devices. A number of technical limitations for integrated optics technology can be mentioned:

- Electronic circuits can consist of very small wires, whilst the geometry of the optical waveguides is limited. The dimensions of the waveguides usually cannot be much smaller than the wavelength and propagation properties to a great extend depend on bends.

- Optical connections between waveguides are much more complicated and critical to fabrication accuracy.

- Some of the optical components can hardly be miniaturized [3].

Mostly for these reasons, integrated optics field has not reached the level of electronic technology development. One of the applications where optical devices are widely applicable is optical fiber communication. Furthermore, continuous development of silicon photonics allows fabrication of advanced waveguides. The field of optical sensors experienced a strong growth. There are examples of the use of sensors in chemical and biomedical applications, environmental monitoring and many other fields.

1.3 Structure of this thesis

The main topics of this thesis are mask design, data logging using LabView™ and experimental work. The second chapter is devoted to explaining the principle of the Mach-Zehnder interferometer and its temperature sensitivity.

The third chapter concentrates on the characterization and design of the chip, including basic information about the fabrication process and simulation of bending losses. Several layout editors for mask design are compared and reasons for the chosen editor are given. Simulation results formed the basis for selection of optimal waveguide parameters such as rib width, height and core height.

The fourth chapter gives detailed description of the experimental setup and programs that were used to record and analyze the data. Equipment used such as temperature controller and plug-in modules are listed. The methods of gathering data and programs to accomplish data analysis are presented as well.

The fifth chapter shows the temperature dependence measured for three different structures: straight waveguide, balanced and unbalanced Mach-Zehnder interferometers.

Finally, in the sixth chapter the conclusions from the accomplished work and suggestions about future work are given.

Chapter 2

A waveguide Mach-Zehnder interferometer and its temperature sensitivity

2.1 The principle of a waveguide Mach-Zehnder interferometer

One of the most important structures which will be considered in this work is the Mach-Zehnder interferometer. An interferometer is an optical device which utilizes the effect of interference, which can occur when two or more light beams are overlapped or superimposed. The Mach-Zehnder interferometer is named after two physicists, Ludwig Mach and Ludwig Zehnder, who developed it. The starting point is a light source that produces an input beam. The beam splitters (BS) are used to divide it into two separate beams and combine them again (figure 2.1).

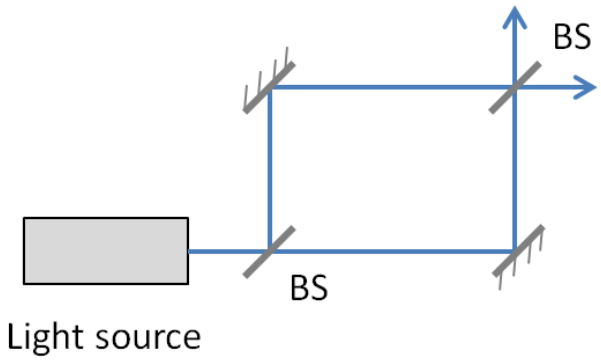

Figure 2.1: Mach-Zehnder interferometer

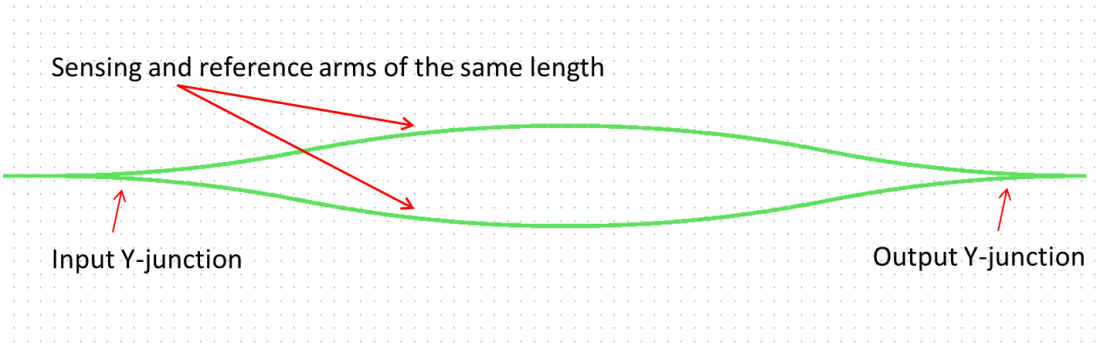

Figure 2.2: Waveguide Mach-Zehnder interferometer

The integrated optical device designed in this project is based on evanescent field sensing: although most of the light is confined within the core of the waveguide, there is a small portion of the guided light that travels through a region that extends outward, approximately half a wavelength, into the medium surrounding the waveguide. This field can therefore interact with the environment. The interaction with the outer medium produces a change in the refractive index at the sensor surface that induces a variation in the optical properties [16].

Different measurement configurations are used to detect this variation, including interferometers. They are used in sensing applications since they can detect the phase variation and measure small variations in the refractive index. For this project, the Mach-Zehnder interferometer (figure 2.2) was chosen due to its high sensitivity.

The waveguide Mach-Zehnder interferometer consists of single-mode optical waveguides and Y-junctions. The light source is a laser. Light is coupled into the waveguide with e.g. a microscope objective with high numerical aperture. The source beam is then divided by a beam splitter. This function is accomplished with a Y-junction that separates the light into two beams of equal intensities. A second Y-junction recombines the two beams, and interference is observed at the output of the interferometer [17].

For sensing applications using waveguide Mach-Zehnder interferometer configuration, the optical waveguides must have two main features: single-mode behavior and a high surface sensitivity.

The first of these two conditions is due to the evanescent sensing approach employed by the sensor. If several modes propagate in the waveguide, each of them detects the variations in the characteristics of the outer medium and the information carried will interfere [16]. The geometry of the waveguide, including core thickness, rib width and depth, and the difference in refractive index between the core and cladding, determines whether the waveguide is single-mode or multi-mode.

At the same time the response of the sensor to changes in the optical properties of the analyzed medium must be as high as possible. As was mentioned earlier, the sensor is based on evanescent field sensing. The concept of evanescent field sensing was initially reported by Lukosz and Tiefenthaler in 1983 [18]. They discovered variations in incoupling angles due to changes in the effective refractive index of the guided modes due to changes in humidity. They also proposed and demonstrated the application of the observed effect towards chemical and biochemical sensing [19]. Single-mode waveguides enable the rapid decay of the evanescent field away from the waveguide surface, which makes them attractive for sensing purposes, because of the minimized background and allows direct analysis of the samples (figure 2.3).

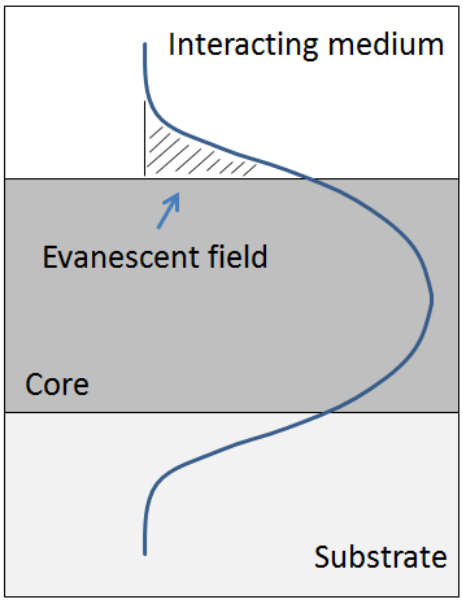

Figure 2.3: Profile of the fundamental mode propagating in the waveguide (not to scale). The highlighted area is a part of the mode traveling in the surrounding medium

As it was mentioned before, in the integrated version of a Mach-Zehnder interferometer, an input beam is split into two beams, which are recombined after a certain distance. Throughout the whole propagation path, the waveguide is covered with a protective layer (cladding), and in only one of the arms a sensor area of length L is opened for contact with the sensing layer. Light travelling in the sensor arm experiences a phase shift, while guided light in the reference arm propagates without changes. At the output of the optical waveguide, the recombination of the light leads to interference. The output intensity can be expressed as a function of the phase difference (Δφ):

$$I = \frac{I_0}{2}(1+\cos\Delta\varphi), \qquad (1)$$

where I_0 is the intensity at the input. For simplicity this expression doesn't take into account propagation losses or differences in the splitting ratio.

The phase difference between guided modes in the reference and sensing arm is:

$$\varphi = \frac{2\pi}{\lambda} L\Delta n_{eff} \quad (2)$$

Here λ is the wavelength in the vacuum, L is the interaction length (length of the sensing area), and Δn_{eff} is the change in the effective refractive index of the mode.

2.2 Temperature sensitivity of a Mach-Zehnder interferometer

The temperature sensitivity of a waveguide Mach-Zehnder interferometer depends on its geometry. In this project we designed two versions: balanced and unbalanced interferometers. In balanced interferometer reference and sensing arms have equal lengths. To investigate the response of these devices on temperature variation, we will examine how the phase difference changes with temperature.

The power source, a laser with 785 nm wavelength, remains the same during the experiments. Thus, the phase difference occurs due to two reasons: thermal expansion of the propagation path and variation in the refractive index of the waveguide. The dependency of the phase on temperature can be derived from equation (2):

$$\frac{\partial\varphi}{\partial T} = \frac{\partial}{\partial T}\frac{2\pi}{\lambda}(Ln_{eff}) = \frac{2\pi}{\lambda}\left(\frac{dL}{dT}\, n_{eff} + L\frac{dn_{eff}}{dT}\right) \quad (3)$$

The phase change can be expressed as:

$$\Delta\varphi = \frac{\partial\varphi}{\partial T}\Delta T \quad (4)$$

The change in the propagation path due to thermal expansion is related to temperature variation by a linear expansion coefficient. It shows the fractional change in length per degree of temperature change. The change in the linear dimension can then be expressed as:

$$\frac{\Delta L}{L} = \alpha_L \Delta T \tag{5}$$

Here α_L is a linear expansion coefficient, and ΔT is temperature variation.

The length dependence on temperature can then be written as:

$$L\,(T) = L_0 + \alpha_L L_0 \Delta T \tag{6}$$

where L_0 is the initial value of the length.

The temperature derivative of the length obtained from equation (6):

$$\frac{dL}{dT} = \alpha_L L_0 \tag{7}$$

The effective refractive index can also be expressed as a function of temperature:

$$n_{eff}(T) = n_{eff} + \alpha_n \Delta T \tag{8}$$

Here n_{eff} is the initial value of the effective refractive index, and α_n is the thermo-optic coefficient of the silicon nitride core.

The temperature derivative of the effective refractive index is:

$$\frac{dn_{eff}}{dT} = \alpha_n \tag{9}$$

Substituting equations (7) and (9) into (4), we get:

$$\Delta\varphi = \frac{\partial\varphi}{\partial T}\Delta T = \frac{2\pi}{\lambda}\,(\alpha_L L_0 n_{eff} + L_0 \alpha_n)\Delta T \tag{10}$$

As it follows from equation (10), the phase difference for balanced Mach-Zehnder interferometer does not exist due to the equal lengths of sensing and reference arms ($L_0 = 0$). If temperature between the two arms is different, it will lead to the phase difference.

The equation is used to calculate the phase difference for unbalanced interferometer, which has L_0 = 1 mm path difference between the arms. The linear expansion coefficient (α_L) of silicon nitride is equal to $3.2*10^{-6}$ $°C^{-1}$[20], and thermo-optic coefficient (α_n) is 10^{-5} RIU/K [21], where RIU is refractive index unit. The intensity of the output power should follow a cosine function given as in equation (1). Substituting these values into equation (10), we find that the phase difference for 10 °C change in temperature is equal to 1.17 rad (67°). Referring to equation (1), this phase difference should cause 30% change of the intensity, provided that the temperature change started when the intensity has the maximum value. However, due to the periodicity of the cosine function and that L_0 is not known with sub-wavelength precision, it is impossible to know if measured intensity I (T_0) starts on top or bottom of cosine function. The intensity change is thus estimated to 30% (1.1 dB) for 10 °C temperature variation, but can deviate from 30% depending on the slope of the cosine function.

Chapter 3

Mask and device design

This chapter describes a waveguides fabrication method, the software used for mask design and design of waveguide elements and devices. In the first section general information about fabrication process is presented. It is followed by the part, which justifies the choice of the software for mask design. The next section explains the importance of waveguide bending losses calculation and reports the results of simulations. The final section gives overview of the waveguide elements and devices available on the chips.

3.1 The fabrication process

Chips used in our experiments were made in Barcelona, and that is why here only general information about fabrication is presented. Processing method that is used in fabricating the waveguides is contact or proximity photolithography. It gives resolution of approximately 1 μm. The method was borrowed from the semiconductor industry where mask lithography is used to pattern the metal on printed circuit boards (PCB). Once the method was well understood, it was realized that mask lithography was also a very useful process for patterning the microstructures.

Photolithography, which is also called “optical lithography” or “UV lithography”, is a process of transferring a prepared pattern from a mask to a light-sensitive material by selective exposure to a UV-light source. The method was originally used in the art world and then implemented in the semiconductor industry where mask lithography is used to pattern the metal on printed circuit boards. The process of lithography used in art is represented by impressing several flat slabs covered with various colors of ink on to a piece of paper. All the layers with different colors should be aligned to each other within a particular tolerance. The advantage of this technique is the ability to produce many copies with high quality.

The first step in optical lithography is to create a mask. A mask is utilized to transfer the designed pattern to a material layer. The mask is typically made by electron beam lithography. There are several steps to accomplish the fabrication: prepare and clean the wafer, cover it with photoresist, expose the resist with light, develop it, etch and remove the rest of not hardened resist from the wafer. After that a substrate, a wafer of glass that is often 100 – 150 mm diameter and about 1mm thick is covered with a layer of photoresist. Photoresist is a polymer that hardens when exposed to light. The wafer with the photoresist is covered with the mask. The light is turned on and the photoresist that is left uncovered by the mask hardens. The wafer, covered with areas of hardened and unhardened photoresist, is put in a solvent which attacks and dissolves the unhardened photoresist. The unhardened resist gets washed away while the hardened photoresist remains on the wafer.

The diagram in figure 3.1 shows the principle of optical lithography. The exposure radiation enters the optical system and is filtered by a mask, which is already aligned with the substrate. All non-exposed photoresist will be removed during development.

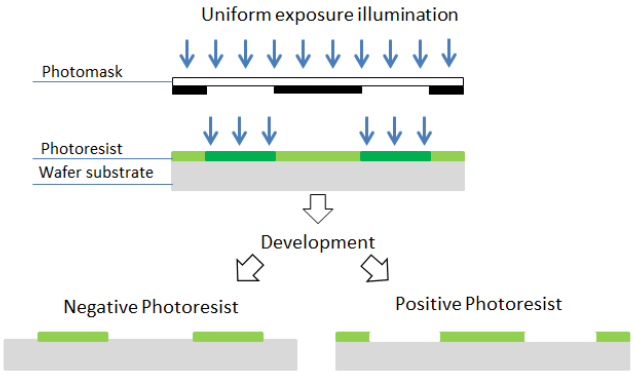

Figure 3.1: Basic outline of optical lithography processes

When the waveguide chip is being fabricated, lithography process includes several steps according to the number of layer in the design. In our case the mask consists of four layers (figure 3.2).

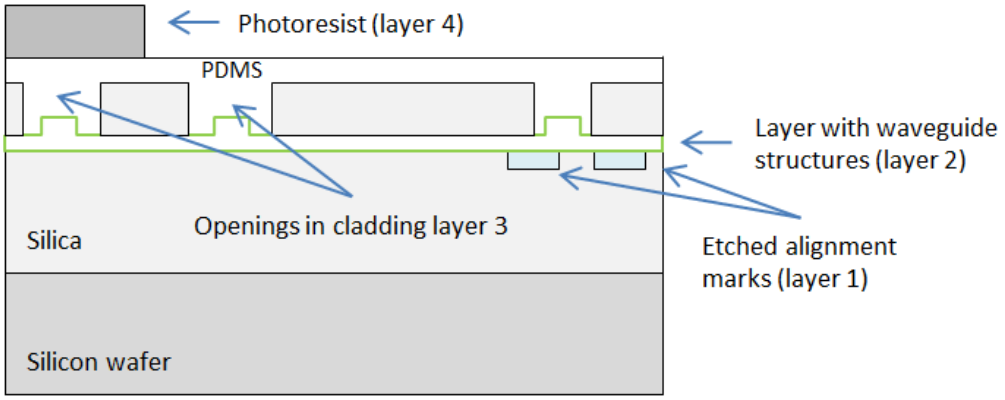

Figure 3.2: Layers of the chip

The fabrication process starts with thermal annealing, when the layer of silica is grown on the wafer. Wafer is a thin slice of semiconductor material, in our case silicon crystal. It serves as a base for further fabrication steps. There are several standard sizes of wafers, for example with 2, 4 and 8 inch diameter. Our manufacturer works with a mask 5 x 5 inches and a wafer with 4 inch diameter. The alignment marks, which are contained in the first layer of the mask, are then etched in silica. All alignment marks presented in next layers are aligned with them. The next step is low-pressure chemical vapor deposition (LPCVD) of

silicon nitride: the pattern of the waveguide structures is deposited on the top of the silica layer. During this step the final geometry of the rib structure is provided: core height, rib height and rib width are key characteristics of this stage. The following phase includes LPCVD of the silica cladding on the top of the previous layer. This layer has openings, so called sensing windows, which allow access to the waveguides. The layer of polydimethylsiloxane (PDMS) then covers the whole surface of the chip. If consider a waveguide Mach-Zehnder interferometer, it has sensing and reference arms, and thus has two openings. One of the sensing windows is covered by photoresist, which does not allow contact between the environment and PDMS layer. Another sensing window gives access to methane to react with methane sensitive layer (PDMS) and influence on light propagation in one of the waveguide arms.

3.2 Software for mask design

In this section several layout editors have been compared, taking into account their user interface and scripting engine. Mask design is one of the most significant steps in waveguide development, and an appropriate layout editor can make the design process flexible and less time consuming. It should also be possible to produce layout files in one of the formats CIF or GDSII, which mask manufacturers accept.

GDS II is a database file format which is the de facto industry standard for data exchange of integrated circuit or IC layout artwork. It is a binary file format representing planar geometric shapes, text labels, and other information about the layout in hierarchical form. The data can be used to reconstruct all or part of the artwork to be used in sharing layouts, transferring artwork between different tools, or creating photo masks. Initially, GDS II was designed as a format used to control integrated circuit photo mask plotting. Despite its limited set of features and low data density, it became the industry conventional format for transfer of IC layout data between design tools of different vendors, all of which operated with proprietary data formats. It was originally developed by Calma for its layout design software, "Graphic Data System" ("GDS") and "GDS II" [22].

CIF (Caltech Intermediate Form) file format was made by Caltech (California Institute of Technology) for describing integrated circuits. CIF

provides a limited set of graphics primitives that are useful for describing the two-dimensional shapes on the different layers of a chip. The format allows hierarchical description, which makes the representation concise [23].

The layout programs for consideration were:

- L-Edit;
- LayoutEditor;
- CleWin5.

L-Edit is a commercial layout editor licensed from Tanner Research Incorporated. It is a screen oriented editor with simple menus for drawing various shapes on different layers. L-Edit supports both GDS II and CIF file standards. It is a paid software with 30 days trial period. Drawing can be performed by choosing different basic element in toolbar or using script.

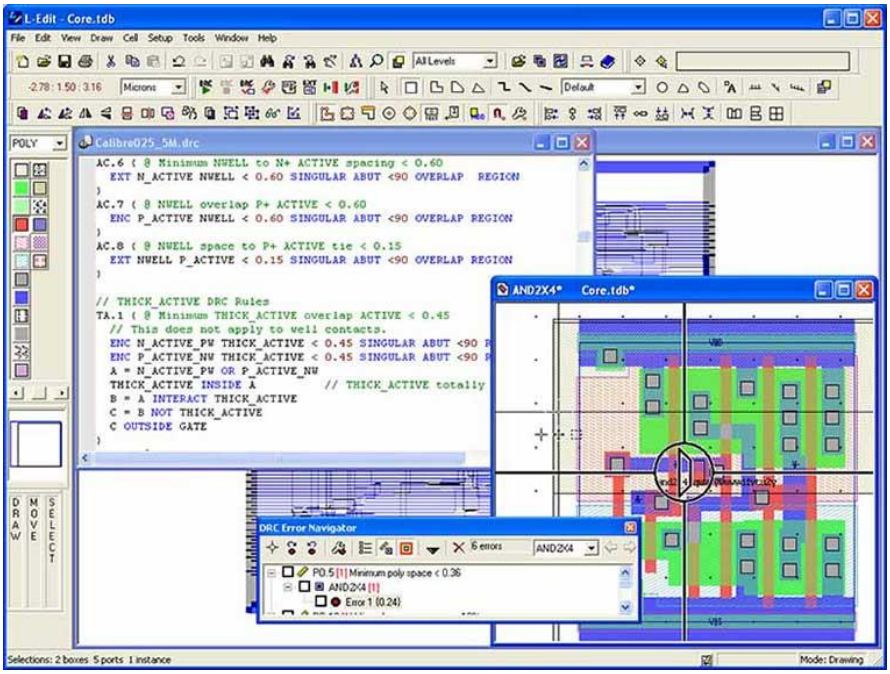

Figure 3.3: L-Edit interface

The interface of the LayoutEditor is equipped with many shortcuts and keys combination to simplify drawing process. The most important handling functions like zooming and scrolling are integrated in each feature and need

not to be called separately. Context menus are available for most parts of the user interface by a right mouse click. The user interface of the LayoutEditor is adjustable. The default appearance (figure 3.4) only includes most imported parts. Further toolbars and sub-windows can be added on demand from the main menu. LayoutEditor supports a wide range of files: GDS II, OASIS, CIF, DXF, Gerber etc. The software is free of charge and can be downloaded from the website.

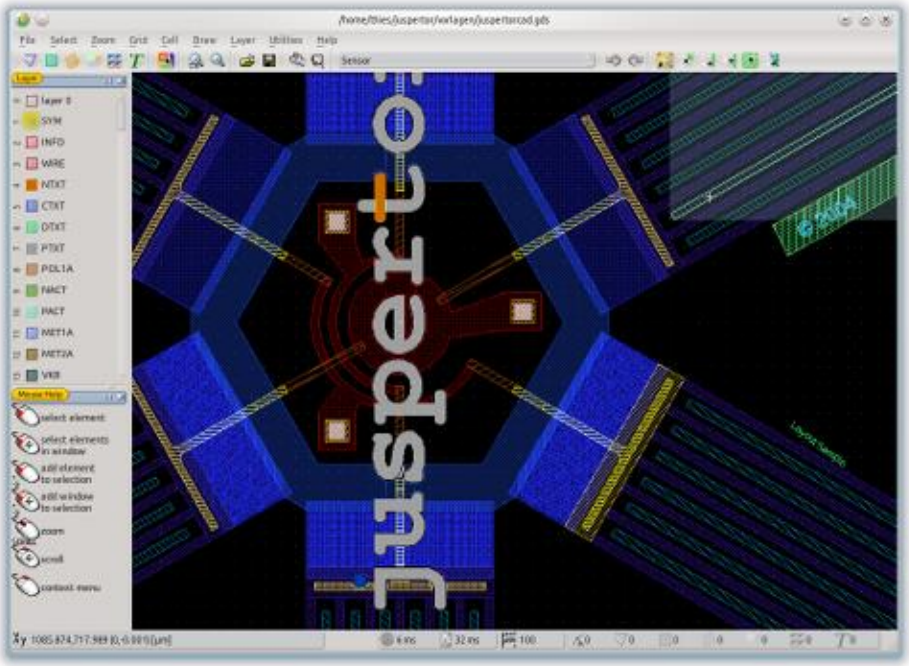

Figure 3.4: LayoutEditor interface

The layout editor CleWin (figure 3.5) is WieWeb software's main product, designed in cooperation with MESA Research institute at the University of Twente and Deltamask, a mask making company. It is compatible with other layout packages since it uses the standard CIF and GDS II file formats, and can read and write AutoCAD DXF format. CleWin is a hierarchical layout editor which means that a layout consists of symbols (also called cells) which may be nested. Editing a symbol in one place will change all other instances of the same symbol. CleWin shows a hierarchical list of all symbols in a design, so that each symbol definition is directly accessible for editing. Furthermore, the hierarchical list provides a clear overview of the file structure and the dependencies between the defined symbols. It has a scripting engine, which

allows the generation of objects using four different languages: C, MATLAB, MaskEngineer language and Lua. Scripts are useful for complex, parametric designs, and for creation of smooth curves or when a variation of a pattern is needed.

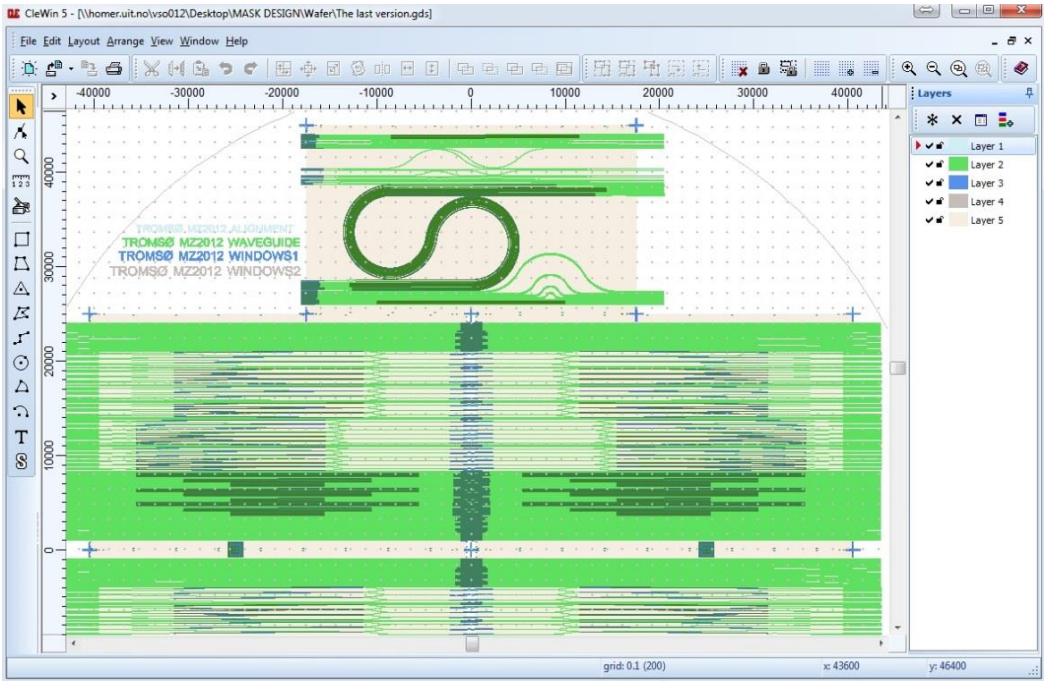

Figure 3.5: CleWin5 interface

All the editors have similar main window (desktop). On the left there is the hierarchy browser which depicts the cell hierarchy. The center panel is the actual canvas where the layout is drawn. Zoom and draw instruments are available there. The right panel usually shows the layer list. Several control panels are available for setting colors, fill and drawing styles. Multiple layers can be shown one at a time or they can be overlaid.

Finally, CleWin5 was chosen for mask development. The two main reasons for the decision were: user interface and a scripting engine. It was crucial that user interface should be understandable and easy to learn. The scripting engine presented by MaskEngineer allows designing of complicated structures and gives the opportunity to change the structures and parameters very quickly.

As an example, a code for a rectangle in CleWin5 is described using variables. Drawing can be implemented in two ways. The first way implies using a function with numbers for length and width (in μm):

```
ml::Straight (cin -> [0, 0]: wfix (50), 300);
// Function returns a rectangle 50 μm wide by 300 μm long
```

In the second case we set the length and width with two variables – "a" and "b":

```
var a = 50,
    b = 300;
ml::Straight (cin -> [0,0] : wfix(a), b);
// Function returns a rectangle a by b μm
```

Figure 3.6: Rectangle built in CleWin5

The final result in both cases will be the same and is illustrated in figure 3.6. The difference between these two methods is that the second method allows to change variables in the beginning of the code and to eliminate time spent on search and modification. By using MaskEngineer, it is possible to modify the dimensions of the rectangle regardless of where the relevant section is located in a script. It can be useful while using repetitive structures, reducing time consumption.

3.3 Simulation of waveguide bending losses in FIMMWAVE

The first phase of the design process was to decide what kind of structures were going to be used in the experiments. Our mask was planned to have two different kinds of chips: normal and special chips as we named them. Both types include straight waveguides. Moreover, each chip contains structures which consist of many bends: Mach-Zehnder interferometers (MZI), U-bends, buckled MZI etc. Therefore, a bent waveguide is an essential element to be considered in this chapter.

3.3.1 Waveguide bending losses

When waveguide bends are used in the design, it is important to ensure that bending is accomplished in the correct manner. Otherwise, light will not propagate in the required manner, and will cause unwanted loss. In this chapter explanation of bending losses is given based on the book of Donald L. Lee. [25]

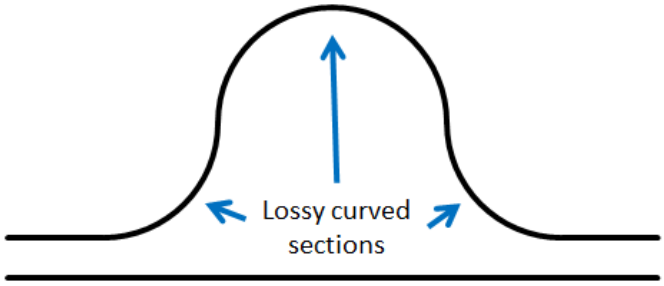

Figure 3.7: U – bend

One of the pathways placed on our special chip is U-bend shown in figure 3.7. This type of pathway leads to changes in propagation direction of the light and as a consequence to changes in power confined in waveguide and radiated away from it. Another type of structure to be designed is the buckled MZI. It consists of two main elements: a Y-junction and a curved section of radius R.

The geometry of the Y-junction is shown in figure 3.8 and can be considered as a serial connection of the following elements: straight waveguide, two bends of radius r and a straight section. Our goal is to find the optimal value of the bending radius taking into account the required distance between two parallel branches represented by the straight waveguides.

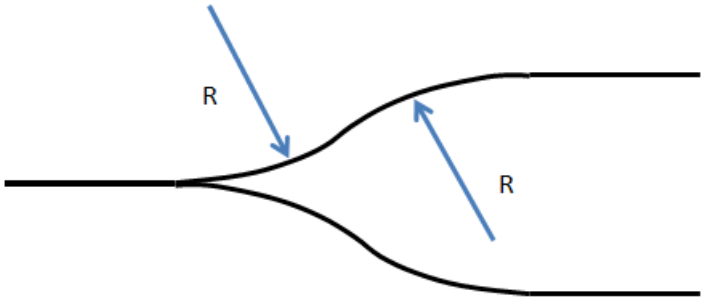

Figure 3.8: The geometry of a Y-junction

To understand the nature of bending losses, consider a curved section of radius R of the waveguide as shown in figure 3.9. The picture demonstrates the top view of a three-dimensional dielectric waveguide. This waveguide consists of a rectangular core of high permittivity ε_2 over the substrate of lower permittivity ε_3. The surrounding region has permittivity ε_1. Guidance for this particular structure is a result of total internal reflection at the interfaces between regions with ε_2 and ε_1.

The propagation direction z of the light is defined to be along the centre of the waveguide. Consider the condition and behavior of the guided wave at two points – when it enters the bend just after the straight section and at some distance from this point on the curved section. It is assumed that the waveguide is operated so that only a fundamental mode is present.

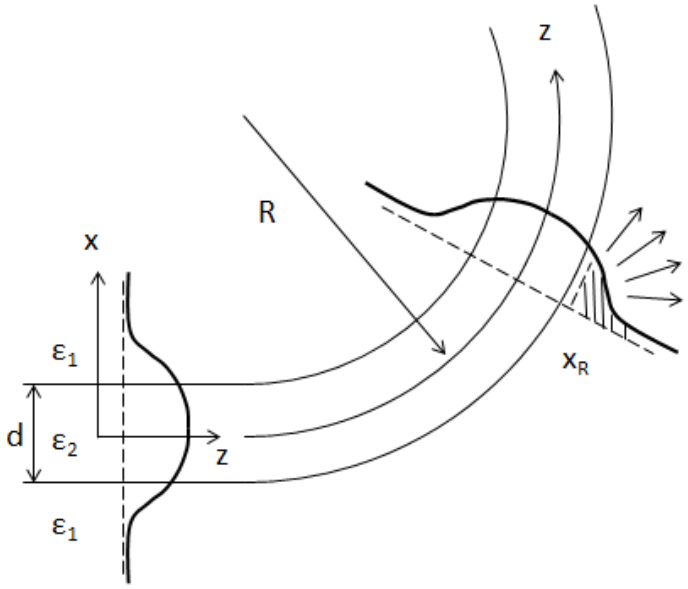

Figure 3.9: Section of a curved waveguide

Regarding the straight section, it can be represented as a curvature with radius R, when R -> ∞. It is known that along the propagation axis of a straight waveguide, the properties of the mode will not vary. If we consider a curved section with a large radius R, properties of the mode should also not differ significantly along the propagation axis. The phase fronts are perpendicular to the z axis, and the field distribution along such a phase front is assumed to be similar to that of the straight waveguide. The phase velocity is the rate at which the phase of the wave propagates in space. If we consider the phase velocity along the waveguide axis, it should approximate that for the straight section. It is given by ω/k_z, where ω is angular frequency, which specifies the number of oscillations per unit of time, and propagation constant k_z, which specifies the number of oscillations per unit of space. This must be equal to the tangential velocity $Rd\theta/dt$ at a distance R from the center of curvature:

$$\frac{\omega}{k_z} = R\frac{d\theta}{dt} \tag{1}$$

Let us turn to points on the constant phase front which are further away from waveguide, and consider the tangential velocity of these points. All of them are included in the same phase front and therefore have the same

angular velocity dθ/dt. Tangential velocity depends on the distance from the center of curvature and is equal to $v_{tan} = (x + R)\, d\theta/dt$. It has a linear dependence on the distance x from the waveguide axis. When x increases there is some point x_r where the tangential velocity will exceed the velocity of light in the surrounding medium, region 1. This point can be expressed as:

$$\frac{\omega}{k_z} = (x_r + R)\frac{d\theta}{dt}, \tag{2}$$

where

$$k_1 = \omega\sqrt{\mu\varepsilon_1}. \tag{3}$$

To express x_r in terms of the waveguide parameters, equations (1) and (2) are combined:

$$x_r = \left(\frac{k_z - k_1}{k_1}\right) R = \left(\frac{n_{eff} - n_1}{n_1}\right) R. \tag{4}$$

Referring to the figure 3.9, x_r can be interpreted as a border. Beyond this distance from the waveguide axis some part of the evanescent field is not able to travel quickly enough to remain in phase with the rest of the guided mode. Therefore it must be radiated away into surrounding region 1. It does not entail that no field exist after the power is radiated at the point z = 0. On the contrary, it is continually supplied with power from the guided mode. This leads to decreasing amplitude of the mode as it propagates around the bend.

3.3.2 Simulation of bending losses in FIMMWAVE

A short analysis is given using the software FIMMWAVE to evaluate appropriate geometrical parameters of the bent rib waveguide such as the radius of curvature, the rib width and height. FIMMWAVE is a fully vectorial mode finder for 2D and 3D waveguide structures, which can be made of any material and of almost any geometry. Two solvers currently implemented in FIMMWAVE were used.

The FMM Solver, based on the Film Mode Matching Method, is for waveguide structures with a rectangular geometry that can be simply discretized into rectangles. This method models an arbitrary waveguide by a sequence of vertical slices, each uniform sideways, but composed vertically of a number of layers.

The FDM Solver is based on an advanced finite-difference algorithm. It can accurately model waveguides with high-step refractive index profiles, curved interfaces and gradient profiles, and is suitable for applications in silicon photonics devices.

This analysis was performed and will be published soon by a PhD-student, Firehun Tsige Dullo, who is one of the participants in the methane detection project.

The objective of the work was to investigate the dependency of bending losses for shallow rib waveguides on various parameters, including radius of curvature, rib height and width. Knowledge about for example the optimal radius allows integration of more components and functions on the same chip, which requires low bending loss in waveguides. The geometry for simulations is shown in figure 3.10.

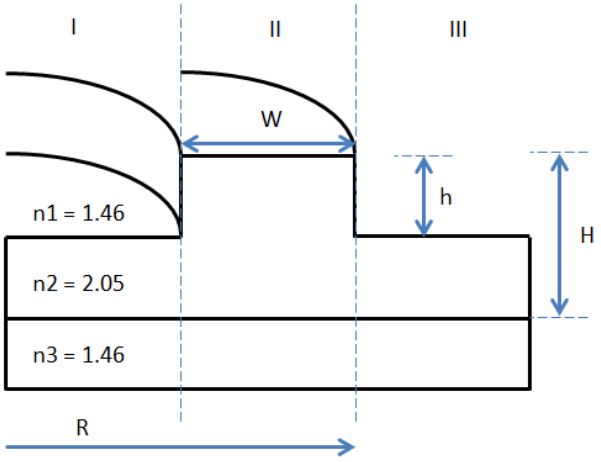

Figure 3.10: Cross section of the rib waveguide

Parameters that characterize the waveguide are: core height H, width of the rib W, height of the rib h and bend radius R. Silicon nitride Si_3N_4 with refractive index 2.05 is commonly used for sensing applications and was chosen for our project. For the cladding silica (n=1.46) was used.

The result of the simulations shows that bending losses are strongly dependent on the bending radius (figure 3.11), width and height of the rib. It can be observed that along with increasing of the radius, bending losses are decreasing. And with a better guided mode, for instance in a thicker core, higher or wider rib, bending losses decrease as well.

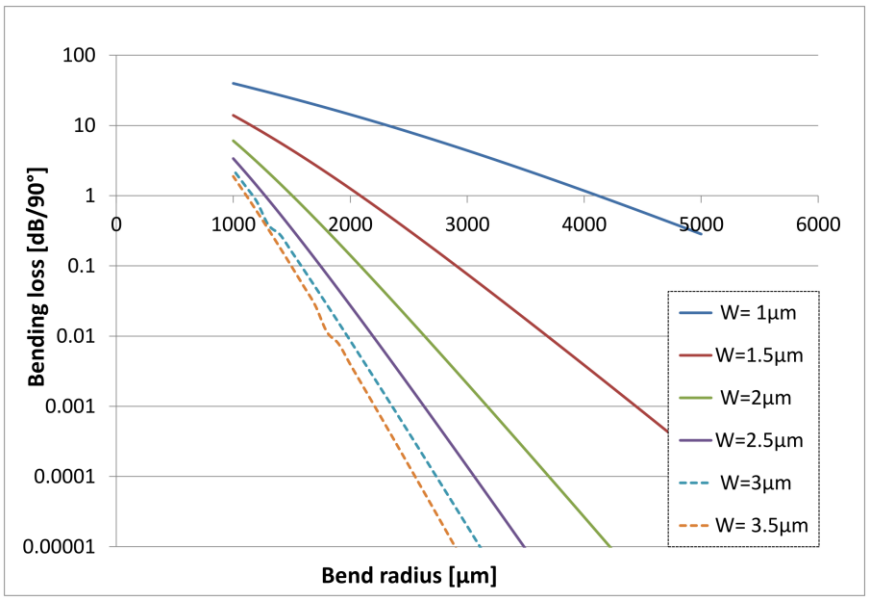

Figure 3.11: Bending loss as a function of the bending radius

The results are presented more intuitively in figure 3.12, where the curve shows the dependence of bending losses on the bend radius for a fixed core height (5 nm). As it can be seen from the figure, with increasing radius bending losses decrease. Several factors have to be considered to choose particular values of parameters for mask design. First of all, it is the threshold of affordable losses. Waveguide should not have high losses. Otherwise it is difficult to obtain reliable result. Secondly, radius must be considered in a matter to have as many structures on a chip as possible. Increasing the radius it is becoming more complicated to combine several structures together. Having compact and efficient layout is one of the key features that characterize integrated optical devices.

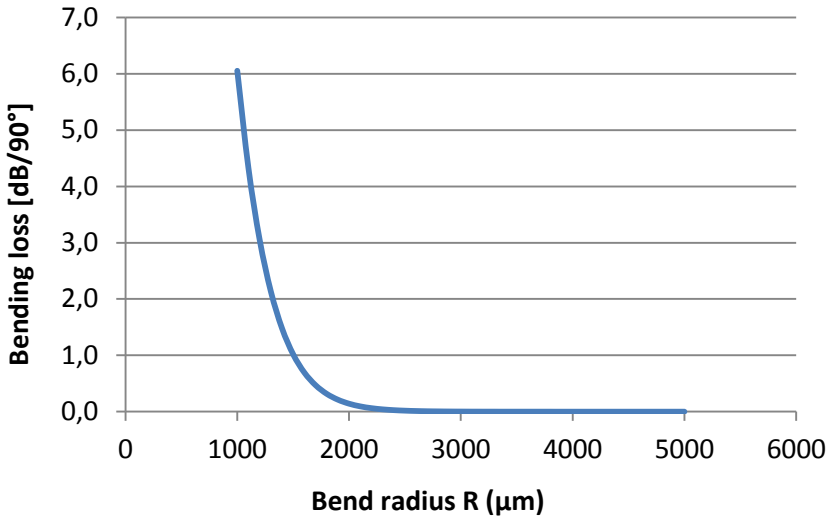

Figure 3.12: Bending losses versus radius

According to the reasons above, the profile of the rib waveguide used in our project was chosen. Waveguides operate in a single-mode; most of the structures have 2 and 3 µm rib width and 5 nm height, while the core height is 150 nm. It was decided to limit radius of curvatures by 4 mm.

3.4 Mask design

3.4.1 Description of the chips

In this chapter the description of the chips is given, including overview of the alignment marks and characterization of the devices.

It was decided to have two types of chips where various structures will be placed, one called “normal” chip, the second type got the name “special”. The normal chip contains basic structures such as straight waveguides, tapers, several Mach-Zehnder interferometers and some other devices. The special chip has unbalanced Mach-Zehnder interferometers, U-bends and buckled Mach-Zehnders.

The starting point for the design was a mask with dimensions 5 x 5 inches and a wafer with 4 inch diameter. The final layout is shown in figure 3.13. The circle has diameter 4 inches, showing the size of the wafer. Inside the circle there are six chips, placed on the wafer. The chips located at the top and at the bottom are special, the four chips in the middle of the wafer are normal. The chip size is chosen for two reasons: the size of the micro-fluidic system and the wafer size. The micro-fluidic system will be used to flow water or gas over the sensor. The normal chip has dimensions 40 mm by 25 mm, while the special is 35 mm by 20 mm. The layout shows layers in different colors. The first and lowest layer (light blue) includes only alignment marks. For the other layers, pattern is etched. The second layer (green) is the core layer (silicon nitride), which contains the waveguide structures. The third layer (blue color) has marks at the beginning of the waveguides. And the fourth layer (brown) is the openings in cladding.

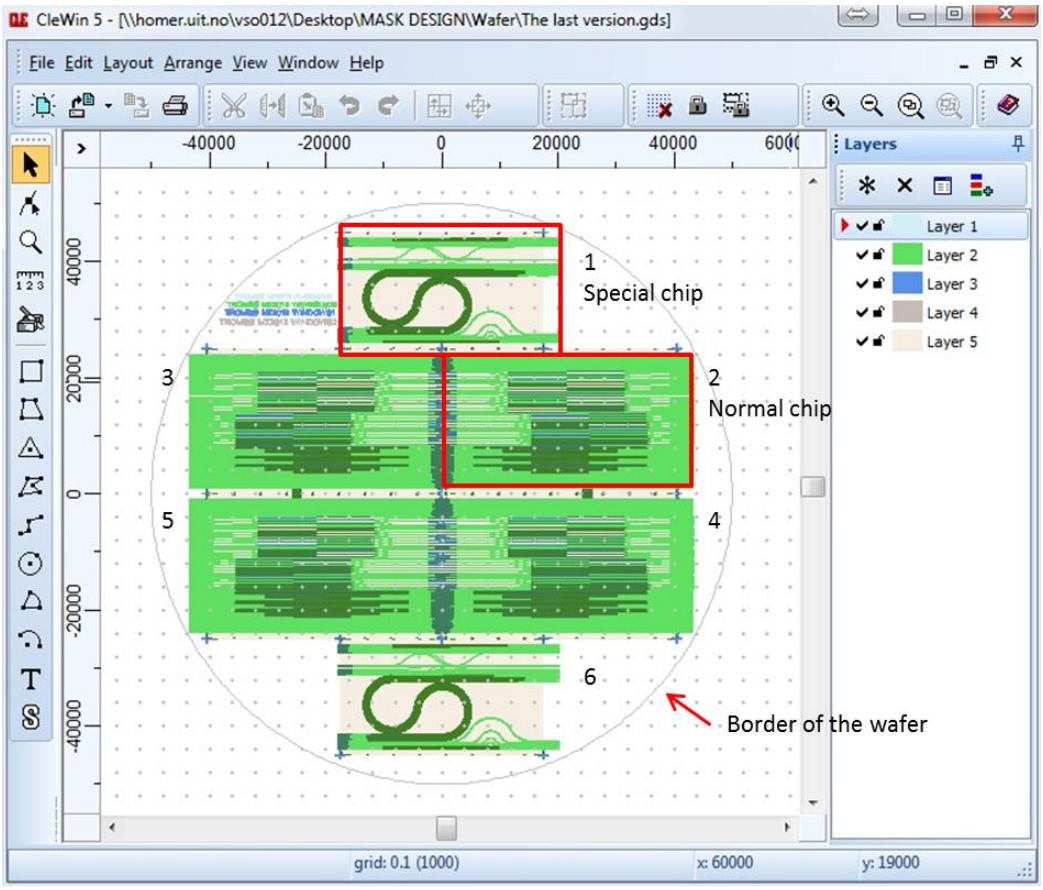

Figure 3.13: The wafer

Each chip has an area free from waveguides on the long sides. The width of this area is 1 mm and the main purpose is to prevent damage of the waveguides while sawing or cutting the wafer. In order to carry out the correct and accurate sawing, the space between chips on a wafer contains alignment marks. The alignment marks for sawing have the form of crosses (figure 3.14) with dimensions 1.5 by 1.5 mm. They are visible to the naked eye or under a small magnification with a microscope. These crosses are etched into the top cladding and were made in the final stage of the wafer fabrication. Otherwise alignment marks would not be visible from the top.

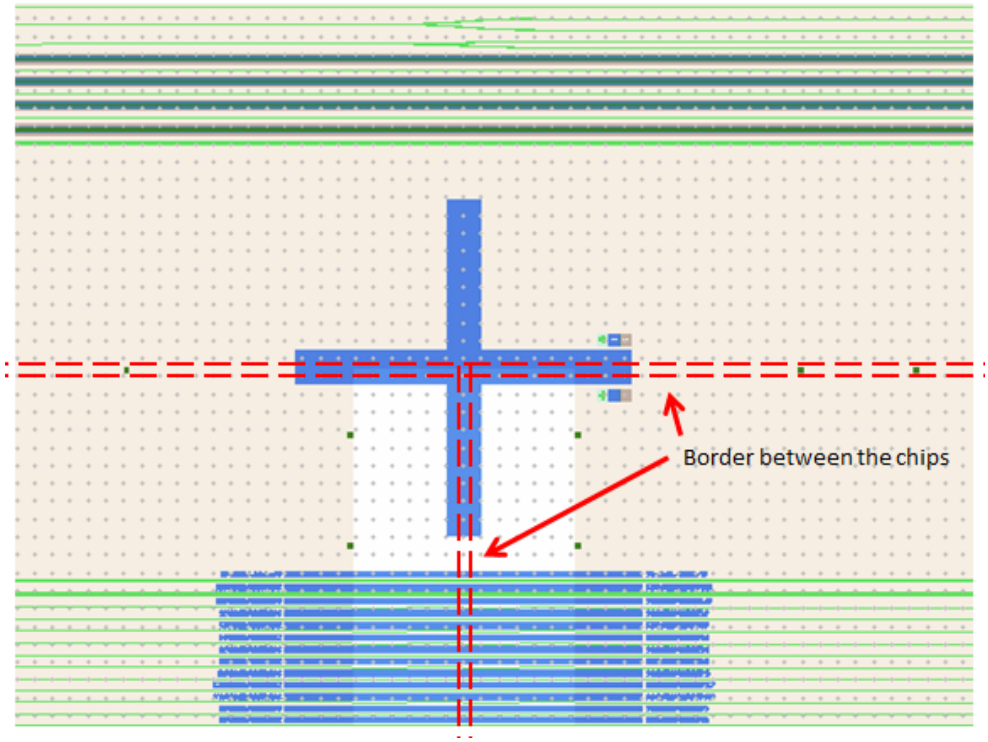

Figure 3.14: Alignment cross for sawing/cutting

The chip also has marks at the beginning of the waveguides (figure 3.15). They are placed in the same layer as crosses for cutting. These marks are essential to identify the position, parameters and type of the waveguide as there is a large number of waveguides, and they are only 5 nm thick (sidewall height).

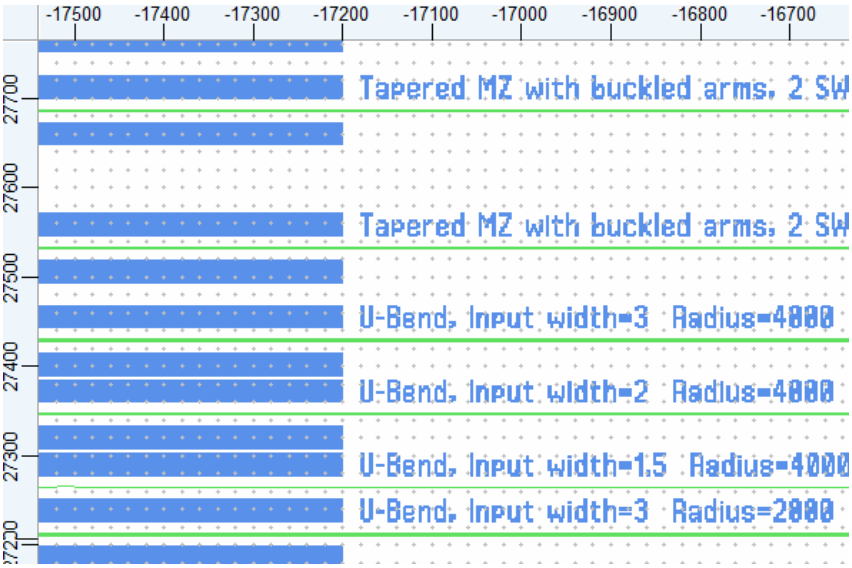

Figure 3.15: Marks (blue rectangles) and text at the beginning of the waveguides

The last type of marks performs the function of aligning different layers in the fabrication process. Before adding a new layer on the top of the previous one, it must be properly aligned. Applying the next mask layer, the alignment marks in that layer must coincide with the same marks in the bottom layer. Figure 3.16 illustrates the alignment marks on the mask.

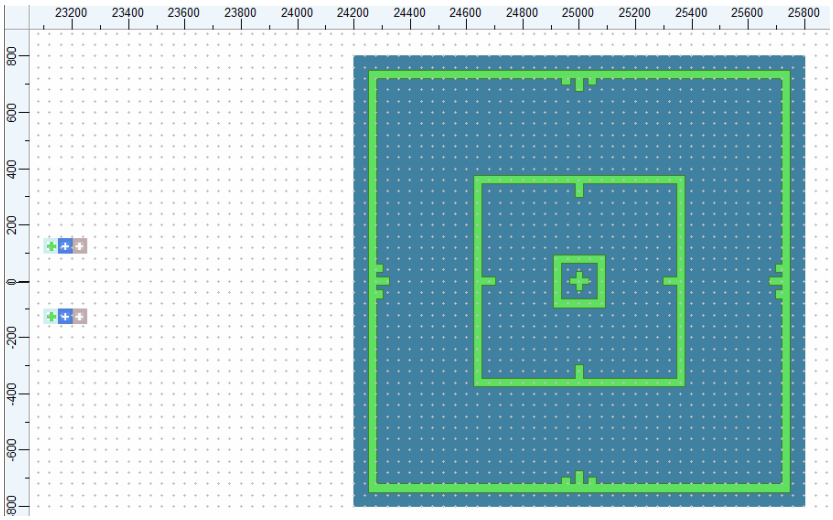

Figure 3.16: Marks for aligning the layers

3.4.2 Design of waveguide elements and devices

For the reason of methane sensing and temperature dependence study several different structures were designed to perform a variety of functions. Straight waveguides are used for checking whether a waveguide is a single-mode or multi-mode. It is possible because of various rib widths from 1.5 µm up to 10 µm. These waveguides can be also used for propagation losses measurement. Balanced and unbalanced Mach-Zehnder interferometers are designed according to the bending losses analysis. Unbalanced MZI serves for temperature study, as it has a difference in a path length between two arms. The main application of normal MZI is sensing of methane when it will be passed through the micro-fluidic system. Some of the devices, as for example U-bends, are designed with different radii to evaluate the results of the bending losses analysis. All devices are placed with minimum 50 µm distance between each other to avoid possible interaction between adjacent elements.

A set of straight waveguides as illustrated in figure 3.17 has two waveguides of each width. One reason for this is uncertainty in fabrication process. Having two waveguides of the same width allows verification of the results obtained from one element on another one. The set of straight waveguides is also repeated several times on the chip. This prevents possible damage of all elements simultaneously.

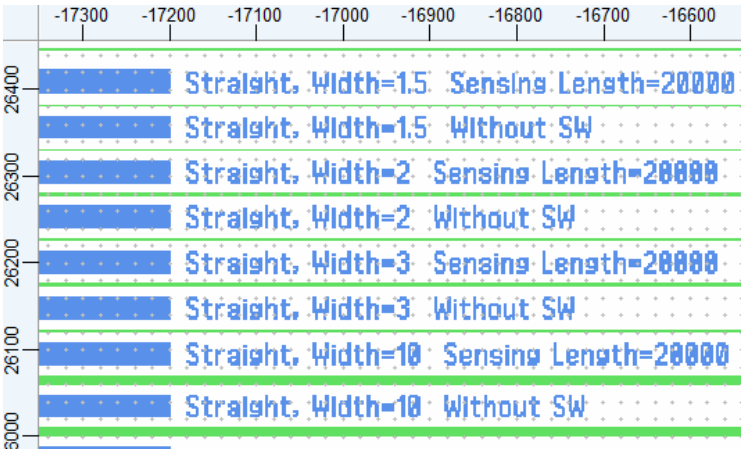

Figure 3.17: Set of straight waveguides

A taper (figure 3.18) is a waveguide gradually expanding from a small width to a larger width. Smooth and gradual expansion allows a fundamental mode to travel from the input section through a tapered part with only minor modifications. This enables the single mode output from the waveguide.

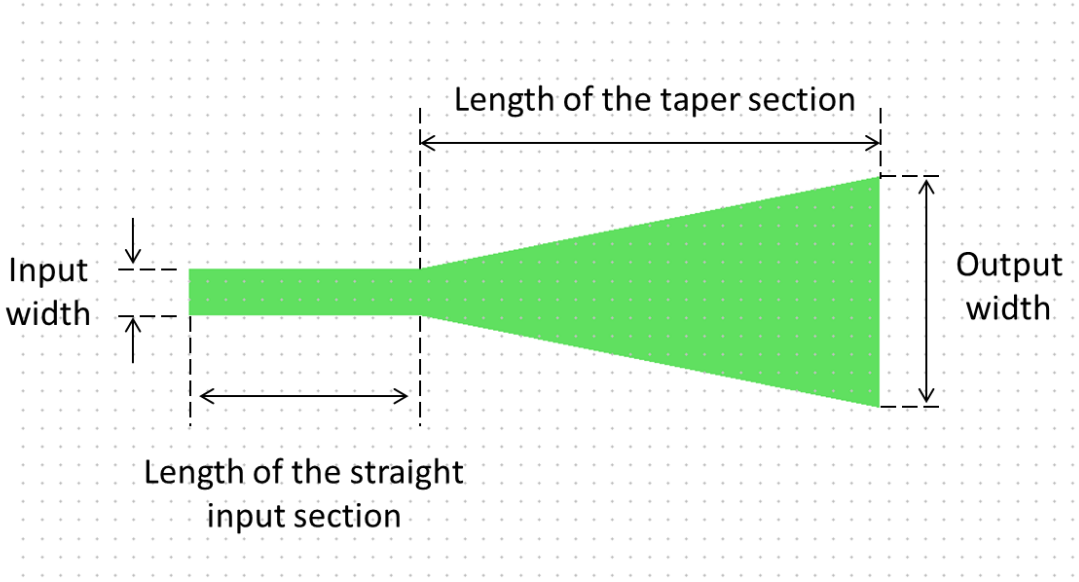

Figure 3.18: Waveguide taper

To construct the taper in the layout editor CleWin, several parameters must be chosen. These parameters are width of the input section and its length, and also length of the tapered section and its output width. All of them are defined as variables in the code.

Text following after marks "//" in the code is comments. The code starts with defining the variables:

```
var     InputWidth = 10,    // Width of the straight input section is set to 10 μm
        InputLength = 50,
        TaperInWidth = InputWidth,
        // Input width of the taper section is equal to the width of the previous
        // straight section
        TaperOutWidth = 50,
        TaperLength = 100;
```

The structure of the waveguide taper is relatively simple, and can be configured like:

ml::Straight (cin -> [0, 0] : wfix (InputWidth), InputLength); // Straight section
ml::Straight (last : wlin (TaperInWidth, TaperOutWidth, TaperLength);
// Tapered section follows after the straight input part.

More advanced devices, such as balanced and unbalanced Mach-Zehnder interferometers require more complicated set of parameters and coding. To design, for instance the balanced MZI, which is shown in figure 3.19, the following set of parameters is required: width and length of input and output sections, radius for bends in Y-junctions, separation distance between sensor and reference arms and the length of these arms (sensing length).

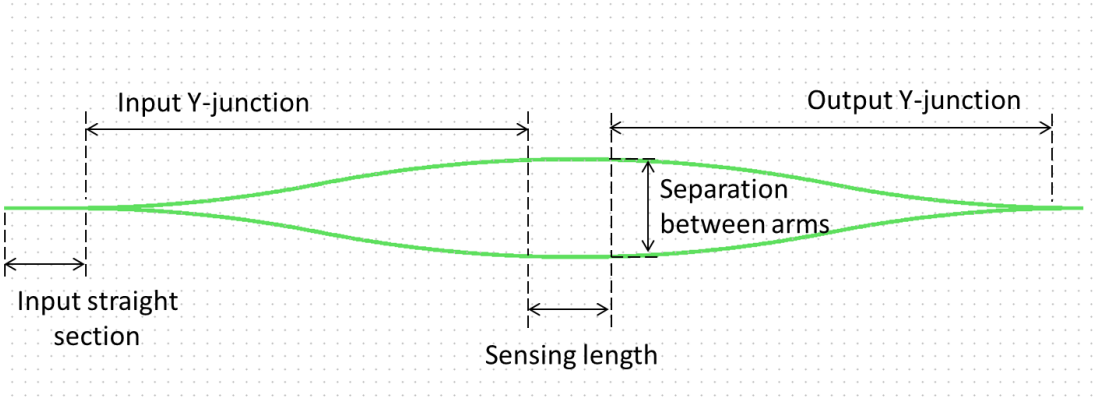

Figure 3.19: Balanced Mach-Zehnder interferometer

One of the most important structures for temperature dependence is unbalanced interferometer shown in figure 3.20. In contrast to a balanced MZI, it contains two arms of a difference length. The difference in path length varies from 1 μm to 1 mm. Small distinction of 1 or 10 μm makes this structure very similar to balanced MZI, and allows to check whether the uncertainty in fabrication of balanced MZI can cause power output change due to change in the temperature. The code for this device is configured in a way, that it requires the same set of parameters as the balanced interferometer, with an addition of defining the path difference between the arms. This inequality is configured in the middle part of the device between input and output Y-junctions. The bends in all parts of the device have equal radius.

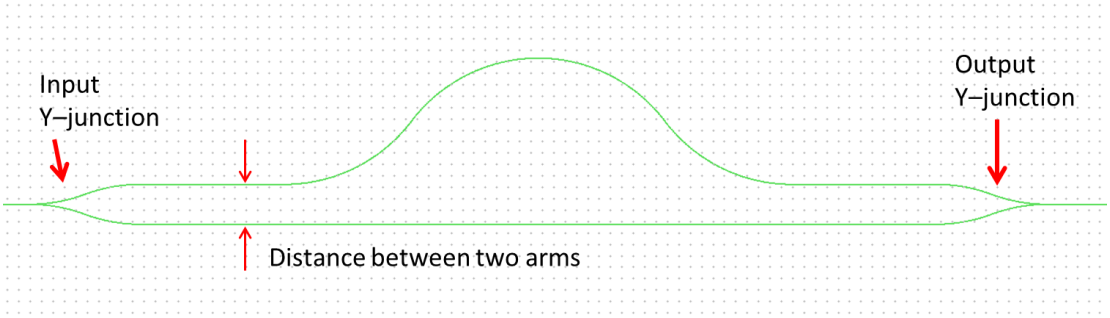

Figure 3.20: Unbalanced Mach-Zehnder

A waveguide configured in a form of U-bend, which is shown in Figure 3.21, is a series connection of four curved sections starting and ending with straight waveguide sections of a certain width. Radius of the rounded sections was chosen from 500 µm up to 4000 µm in order to check the simulation results of bending losses. For each radius value there is a set of three waveguides having 1.5 µm, 2 µm and 3 µm width.

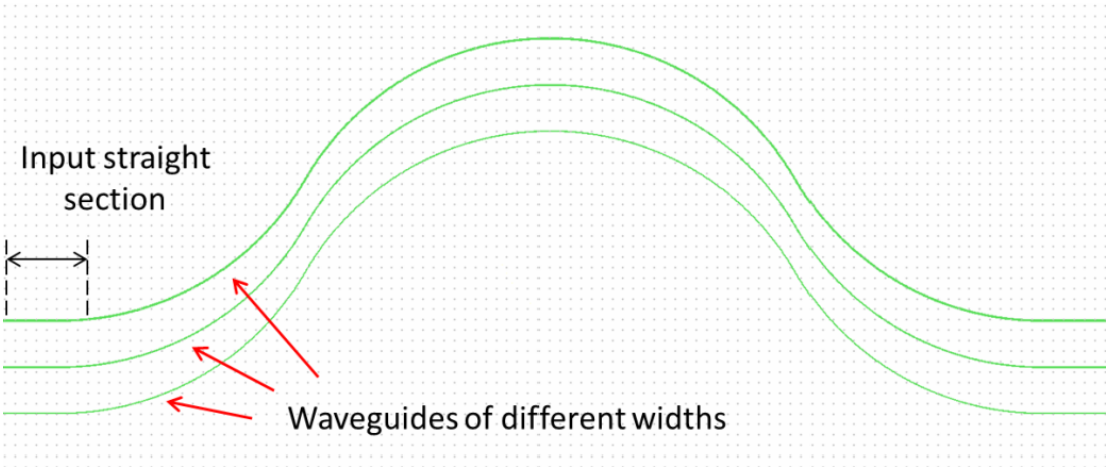

Figure 3.21: Set of U-Bend waveguides with different widths

On the special chip there is also a structure, called buckled Mach-Zehnder, obtained by modification of the balanced interferometer. It starts with the same Y-junction at the input, and ends with Y-junction at the output. The difference is that it has longer arms, which increase the sensitivity of the device. Opportunity to have elongate straight sensing areas is limited by the length of the special ship. In order to increase the length, structure is curved as

shown in figure 3.22. Radius of the curved section is chosen to be 4 mm according to the results of bending losses simulations. Maximum achieved length of the sensing openings is 80 mm.

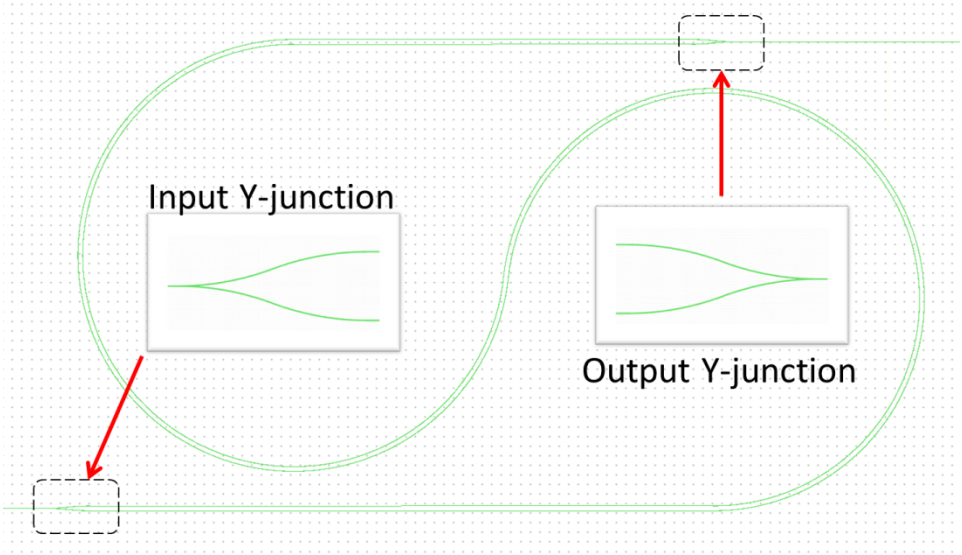

Figure 3.22: Buckled Mach-Zehnder

Chapter 4

Experimental setup and gathering of data

4.1 Overview of the setup

In this section the experimental setup is described. The description is separated into three sections. These are optical components, microscope and lasers. Adjustment of the beam size by arranging the lenses is considered, followed by specification of camera used in conjunction with a microscope and specification of the laser. A schematic view of the overall setup is shown in figure 4.1.

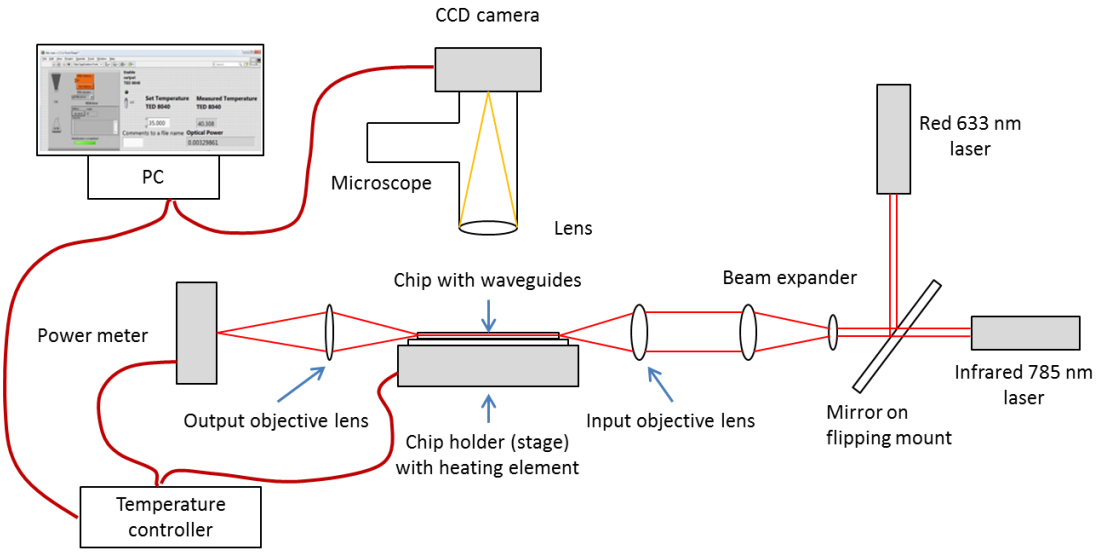

Figure 4.1: Schematic diagram of the experimental setup used for temperature dependence study

4.1.1 Optical components

The laser used for temperature dependence study has a wavelength of 785 nm. During the alignment process the output beam from the red laser with a wavelength of 633 nm is redirected by a mirror mounted on a flip stage and sent into one of the lenses intended to expand the beam. When alignment is finished, the flipping mirror is repositioned outside the beam path and setup is ready to be used with the main laser.

The beam then passes through two lenses in order to expand it to match the input of the objective lens. This 40x input objective lens couples the beam into a waveguide. It is necessary to expand the beam because the diameter of the 785 nm and 633 nm beams are 1.1 and 0.8 mm, respectively, whereas the entrance diameter of the objective lens that couples light into a waveguide is 5 mm. It means that magnification of 4x is required. In order to fit

the diameter of the laser beam and lens diameter a Keplerian beam expander was constructed (figure 4.2).

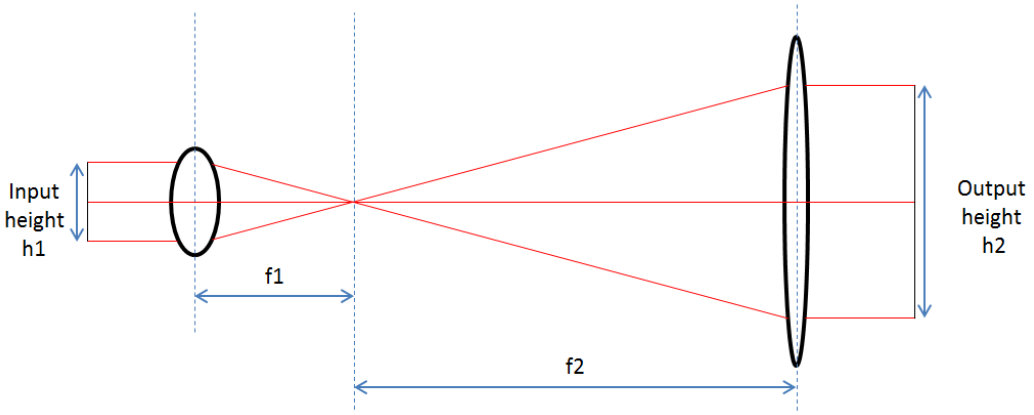

Figure 4.2: Keplerian Beam Expander

Two lenses with positive focal lengths are arranged at a distance f1 + f2 [25]. The magnification M of the beam expander can be found as:

$$M = \frac{f_2}{f_1} = \frac{h_2}{h_1} \tag{11}$$

where,
f1 – effective focal length of the input lens
f2 – effective focal length of the output lens
h1 – diameter of entry spot
h2 – diameter of exit spot

Using lenses with focal lengths 150 mm and 35 mm, the magnification is equal to 4.285 and corresponds to the required value. Lenses are placed at a distance of 185 mm.

A piezo controller (figure 4.3 a) in combination with a 3-axis flexure stage (figure 4.3 b) was used to achieve precise coupling. The unit has three piezoelectric actuators built into the housing to give independent adjustment of each axis. Utilizing this driver gives the opportunity to adjust the stage with the objective lens in the nanometer range.

a) b)

Figure 4.3: a) Piezo controller b) 3-axis flexure stage system

The 25x output objective lens focuses the output beam from the waveguide on a photodetector. This makes it possible to measure the guided power with a sensitive power meter connected to the Thorlabs PRO8 mainframe.

4.1.2 Microscope

A microscope is used for aligning the input beam and gathering images of the guided light and the waveguide. A CCD camera (uEye) is connected to the microscope (figure 4.1). A white light source allows it to work in bright field mode with white light incident on a waveguide and reflected. This mode is used to find the required waveguide on a chip and to align the focused spot of the input beam with the waveguide. When the light source is switched off, only scattered light from the waveguide strikes the camera. Brighter images can be acquired by changing the exposure time of the camera. A 4x microscope objective is used to observe the waveguides. Moving the microscope is possible in all three dimensions and allows focusing on the chosen waveguide.

4.1.3 Laser

Two lasers are used in the setup as shown in figure 4.1) A red laser with wavelength 633 nm is used for preliminary alignment and focusing of optical components. It is placed perpendicular to the main optical line of the setup. This laser has a low power output and serves only as a guide while adjusting because its light is visible.

The laser source used for temperature dependence study is an infrared diode laser with 785 nm wavelength. It has an output power stability of 0.03 dB. Maximum value of the optical power measured at the output of the fabricated waveguide is 4 mW, while the output power of the laser initially is 120 mW. The absolute value of the power obtained from the laser is not critical, the most important is its variation with time and ambient temperature.

4.2 Data acquisition and processing

As in every experimental work, the acquisition and processing of the data is an essential step. For the purposes of our experiment, time, temperature, input power and output power from the waveguide were recorded. The latter was measured with a photodiode connected to the PRO8 mainframe. A LabView™ program was developed to acquire this data and a MATLAB program to import and process data from the camera. These programs will be described in this chapter.

The data is stored on a PC during the experiments and analyzed later. The real time processing of the data is not performed due to usage of two independent programs.

4.2.1 Temperature control system and the characteristics of PRO8000

One of the most significant components in our research is a system that controls the temperature of the waveguide chip. This system consists mainly of two parts: a temperature controller and a thermoelectric cooler with feedback given by a temperature sensor.

As a controller, a modular test and measurement system, PRO8000 series, was selected. The main features that were taken into account when choosing the system are:

- Ability to mount several slots (up to 8) in the same rack. This option is useful because power measurement and temperature control modules are able to function simultaneously. Moreover, the extended rack can be used for several experiments.
- Existence of various modules, including two that were used in this project.
- Remote control via IEEE-488 connection with drivers for LabVIEW™. It gives opportunity to create a program that meets our requirements.

Figure 4.4: PRO8000 series modular controller

The PRO8000 Controller is a platform that operates with various modules of electrical and optical functionality. For our application, an 8-slot

chassis was chosen. The first of the installed modular devices is photocurrent measurement module (PDA). The other two are laser diode temperature control modules (TEC).

To measure the output power from the waveguide, a photo current module for PRO8 series was chosen. It has several features:

- 7 Current Measurement Ranges from 10 nA to 10 mA DC.
- High accuracy (±0.025%) of Full Scale Reading.
- Dual channel version.

The latter is very useful for our setup as in the project for subsea sensors two experimental setups will be installed: for detecting methane in air and in water. The appearance of the device is shown in figure 4.5.

Figure 4.5: Photo current module

Optical power can be read-out directly from the module when using it with calibrated photo diodes. After connecting the photo diode, information about measured power is accessible on the main screen of the mother rack. Data from the photo current module is transferrable to personal computer via an IEEE-488 interface. An adapter from IEEE-488 to USB was used to connect the controller to a PC.

On the front panel of the module there are two input channels with BNC connectors, error indicator, indicator which shows that the current module is chosen and an element to adjust the offset after connecting the photo diode to the BNC jack.

In the same manner as PDA module, a temperature control module is a plug-in module for the PRO8 platform. The main function of the module is to provide a stable temperature. The main features of the temperature control module are:

- Wide temperature control range: from – 12.375 up to 90.000 °C
- High temperature stability: <0.002 °C
- Versions with different current ranges: ±2 A for 16 W, ±4 A for 32 W, ±8 A for 64 W. In our project, a 4A limited module was utilized
- Variety of sensors: Pt 100, Pt 1000, thermistors AD590, AD592

The current limit of the module can be adjusted by a potentiometer on the front panel (hardware limit) shown in figure 4.6 or by software, which gives a guarantee that the temperature control module is prevented from damage. All the settings are automatically recorded in memory and recalled when switching on the mainframe, as long as the module was not moved to a different slot.

Figure 4.6: Front view of the TEC module

For our purposes, a thermistor for temperature sensing was chosen for several reasons. First off all, usage of it is possible after short calibration process and setting calibration parameters into the PRO8 platform. Another reason is the size of the sensor. The initial idea was to insert it into a plate, on top of which the waveguide chip would be placed.

As the heating unit a Peltier element has been chosen (figure 4.7). The connection to the temperature controller is made with help of two power

wires. The principle of work is based on the Peltier effect which creates a heat flux between the junctions of two different types of materials. Thus one of the sides is hot, while another is cold. Temperature is adjusted by amperage passing through the element.

Figure 4.7: Standard Peltier element

Another device used in our experiments is a polyimide thermo foil heater (figure 4.8). In our case, it has a size of 44.5 mm by 44.5 mm and the total thickness of less than 1 mm. The heating film is a thin foil made of polyimide with an integrated lattice of metal which conducts current. When current is applied to the film, it generates heat in metal tracks. Polyimide is a thin, semitransparent material that covers the metal wires. In contrast to the Peltier element, the heating foil does not support the change of the current flow direction. Due to this reason the foil is connected to a separate power source.

Figure 4.8: Heating foil

4.2.2 Development of the LabView™ program

The program is the interface between the controller and the researcher. The measured values are displayed on the main screen of the controller. However, research needs to have systematically stored data in a convenient form for processing. Thus, the main functions of the developed program are recording and ease of accessibility to the information afterwards.

The platform PRO8 delivery includes the drivers for the development environment LabView™, which makes the process of writing a program less time consuming. In addition, they allow one to develop software in the presence of basic knowledge in programming and LabView™.

All programs, or virtual instruments (VI) as they are called in LabView™, consist of two windows: the front panel, which contains all the control elements and indicators (figure 4.9), and the block diagram with logic elements and components directly communicating to the mainframe.

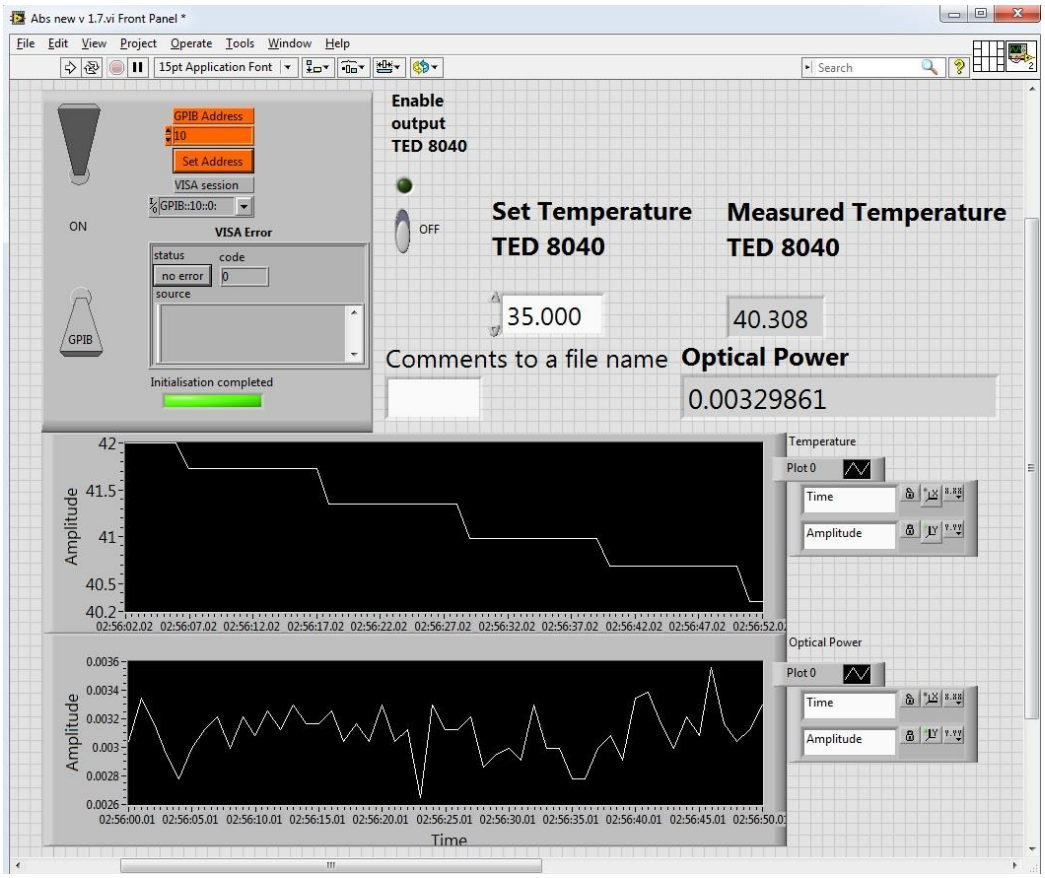

Figure 4.9: Front panel of the LabView™ program

The front panel consists of a start button, program indicators which show in real time the temperature and the measured power, and corresponding graphics. It also includes turning on and off the temperature control module and set its desired value. All data from the program is stored in the predetermined data folder. For ease of identification, comments such as the type of waveguide can be added in the file name before recording the results.

The LabView™ code is visual and shown in figure 4.10. The launch of the program begins with the initialization of the connected device. After that there is an alternate communication with the two plugged in modules and collecting information from them.

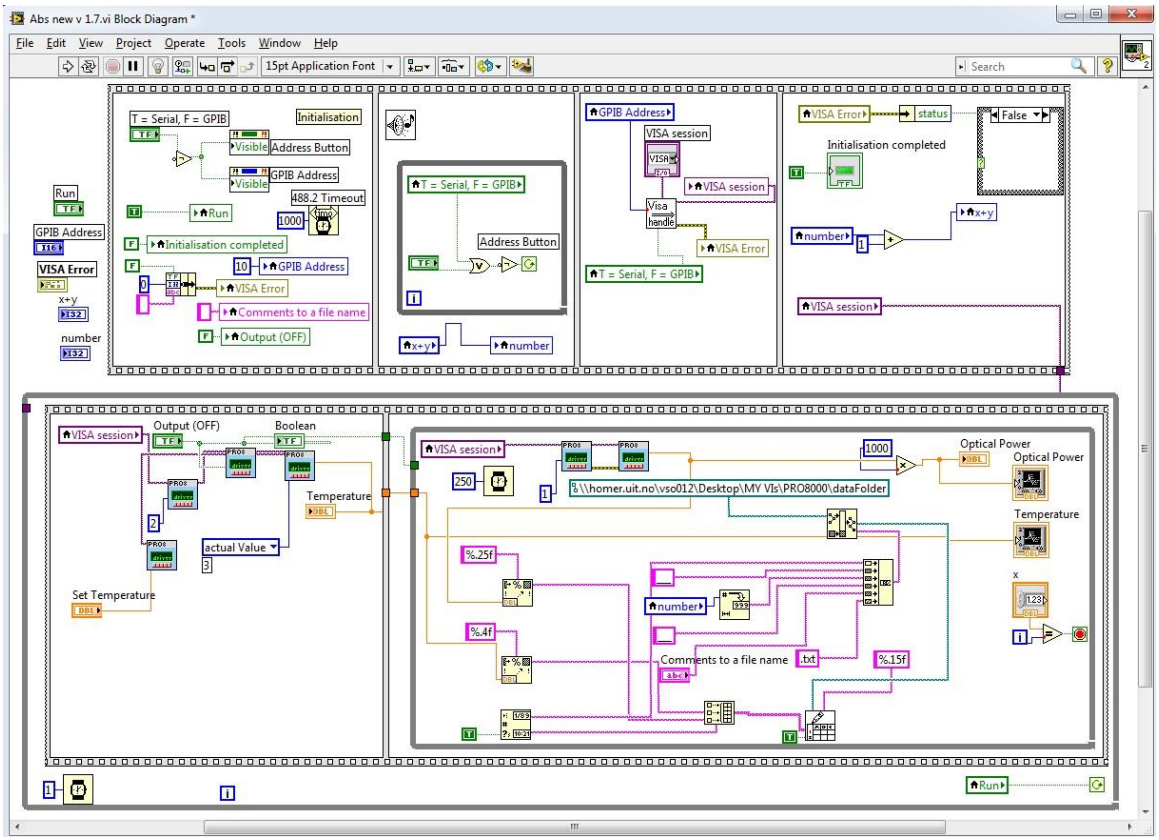

Figure 4.10: Block diagram of the LabView™ program

When the information has been collected in the process of operation, it is written to a file in a pre-selected folder on the hard drive. The block diagram for the data recording is shown in figure 4.11. Therefore, the following information will be displayed in the destination file: the time at which measurement is made, temperature and power.

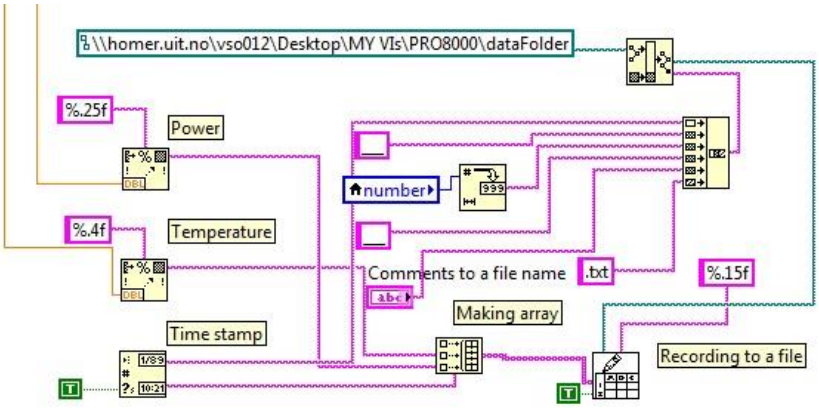

Figure 4.11: Data recording

4.2.3 Reference power measurement

To reduce the influence of noise on the experimental data, a reference power measurement was implemented. It was done to compare the output power from the waveguide with the power coupled into the waveguide. The output optical power P_{out} was measured with a photo detector connected to the power meter module. The data was collected using the developed LabView™ program. The power coupled into the waveguide (P_{ref}) is measured with the camera. Normalized power values (P_{rel}) are then defined as:

$$P_{rel} = \frac{P_{out}}{P_{ref}} \tag{12}$$

Normalized power indicates how two values correspond to each other. The procedure used to measure the input power is shown in figure 4.12. The first step is to find a good coupling using a piezo stage for the input objective lens. The camera captures scattering from the waveguide and record a video file, which includes the changes in the input power. The video file is then converted to a sequence of images, which allows obtaining values of the power input for each second. Afterwards, the images are imported into a developed MATLAB program. The program is developed by Firehun Tsige Dullo, who is a PhD-student working on the methane sensing project. To extract the power values, the program analyses the imported images by choosing certain region of the waveguide and converts the brightness level into a number. These

numbers are compared and normalized with each other. The final step is to plot the power versus time.

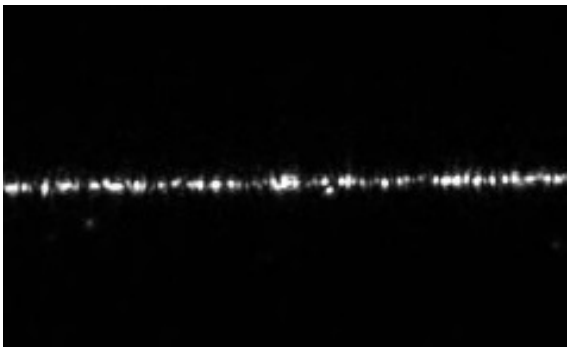

a. Acquire an image of good coupling in the waveguide

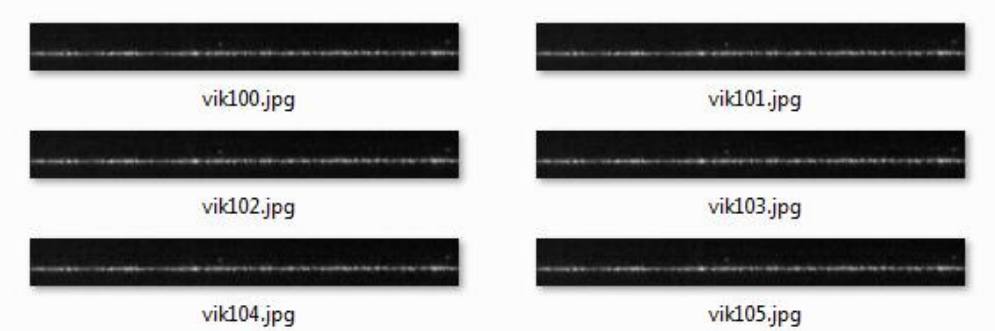

b. Collect data with changing power

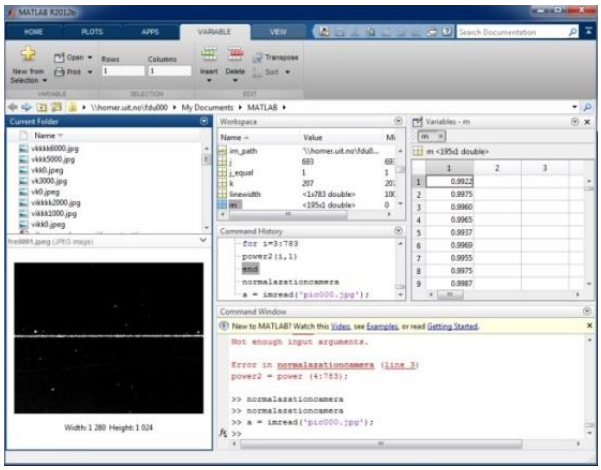

c. Import images into MATLAB

Figure 4.12: The procedure for input power characterization

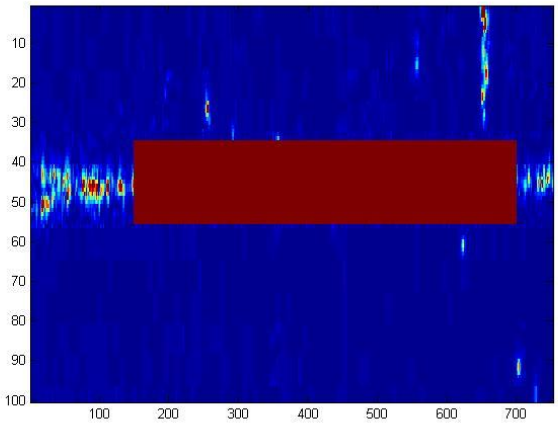

d. Allocate a region for processing

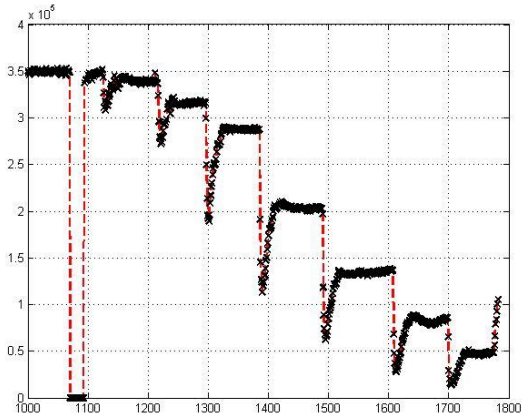

e. Plot power vs. time

Figure 4.12: The procedure for input power characterization

At the start of each experiment, various camera parameters must be adjusted. These are:

- the exposure time. This is the length of time when the camera keeps its electronic shutter open and allows the light to fall on the image sensor. One of the main aspects here is saturation. In order to receive reliable data this must be set such that the brightest pixel is not saturated. For the brighter image the shorter exposure time is required. The adjustment was done by taking histogram into account.

- the region of interest. It is possible to specify a rectangle of pixels that will be converted into a video file for further processing. This reduces the size of the file to be transferred to the PC, thus less time will be spent on processing.

- the frame rate. This is the rate at which images are recorded. In our case, it can be interpreted as the number of values taken per second.

The camera control is performed with a program supplied by the camera's manufacturer. The sequence of images is automatically converted into a video file and stored in a user-defined folder.

In order to change the input power step by step, it was initially proposed to use a polarizer between the laser and the objective lens. The light from the laser is polarized. The intention was to rotate the polarizer from the original position when the throughput of the polarizer is maximum and to move towards decreasing power transmitted through it. The result that was obtained after the experiment is shown in figure 4.13.

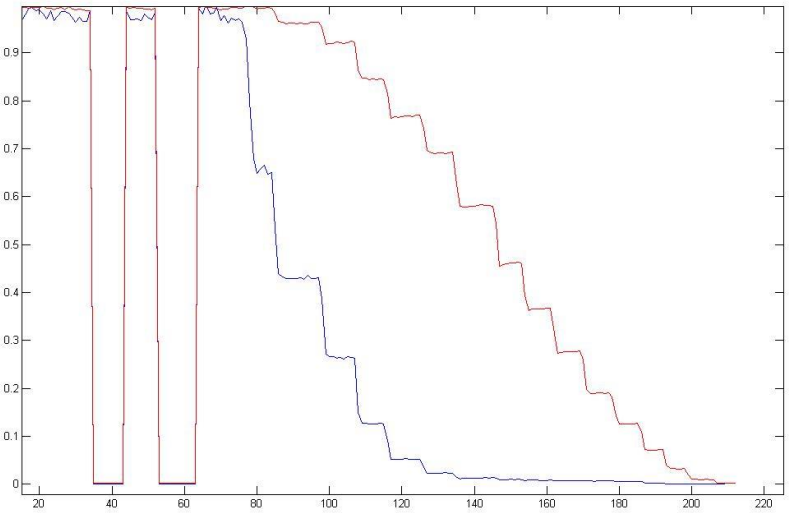

Figure 4.13: Comparison of the input and output power using a polarizer

In figure 4.13 power obtained from the camera is in blue color, from the output – in red. There is a clear mismatch between them. In order to be able to compare these two quantities, one of them should be shifted relative to the

other. Reference points in this case are blackouts which are clearly discernible from the rest of the data. These dips were made by blocking the incident beam before the objective lens. Difference in time between input (reference) and output power exists because recording of the data in LabView™ program and camera software cannot be performed absolutely at the same moment of time and that is why it needs to be adjusted.

The reason for the result in figure 4.13 is that when rotating the polarizer not only the transmission of the polarizer is changed, but polarization of the transmitted beam is also rotated. Vertical and horizontal polarizations of the input beam give different coupling and as a consequence, difference in input and output power values.

The method which led to the intended result is the following: to pull back the objective lens relative to the waveguide. When moving the lens from the chip, the spot on the waveguide input facet becomes wider. Together with the change in the power it gives assurance that the rib of the waveguide is within the coupling spot. After switching to this method the result shown in figure 4.14 was obtained. The power obtained from the camera is marked blue, while the power measured at the output is green. On the graph two dips, made by blocking the input light, can be observed. Both input and output power decrease simultaneously, following the same path.

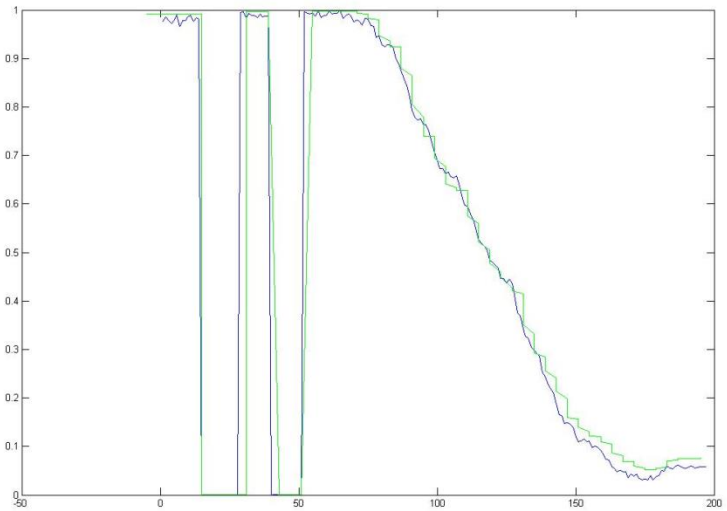

Figure 4.14: Output and input (reference) power measured on straight waveguide by moving the objective away from the waveguide

Summing up the result of this chapter, we found an appropriate reference power measurement method. To ensure the working ability of this method, the input power was gradually decreased with a polarizer, measuring at the same time the power at the input and at the output.

Chapter 5

Experimental results

In this chapter we go through the experimental work done to investigate the temperature dependence of a waveguide Mach-Zehnder interferometer. For better understanding, the experimental work is organized in four phases. First, we studied the output power stability for some time interval at constant (room) temperature to investigate if there is any power output drift without changing the temperature. In the second phase, the temperature varied in order to see if the output power changes with temperature for different waveguide structures. The problem that was experienced in this phase of our experiment is that when we change the temperature, there is a large change in the output power. After several experiments it was observed that the heating system, which was based on a Peltier element, experienced thermal expansion while heating. It resulted in movement of the chip. The chip moves such that the coupling is misaligned, which is the reason that we experienced a large change in power output. In the third phase of our experiment we proposed a method to solve the problem of the previous phase by moving the input objective lens away from the chip to increase the diameter of the beam. Doing this, we reduced the change in the output power. Finally, we changed our heating system to solve our problem

with the chip movement. A heating film was used instead of the Peltier element.

5.1 Power stability

To obtain reliable results in every experiment, any secondary factors affecting the final result must be evaluated and taken into account. Dealing with the light propagation in the waveguides, one of the major factors that influences the output power is coupling into the waveguide. It is also the stability of the output power for constant temperature. This makes it clear whether changes are caused by fluctuations in temperature or any other factors.

The first performed measurements are related to power stability. After proper coupling, the waveguide was left for some time interval without any modifications in spatial position of the chip, coupling or input power, and output power was measured. The duration of the experiments was calculated taking into account a number of conditions. First of all, it should not be too long. It is expected that the intensity of the power output will decrease over time. At the same time the experiment duration should be long enough to allow a gradual increase in temperature which is needed for temperature study. Therefor the time limit was set to ten minutes.

The experiments were conducted with the following structures: straight waveguides including 1.5, 3 and 10 μm rib width, and balanced Mach-Zehnder interferometer with input width 3 μm. The results are presented in figures 5.1 – 5.4. The change in power output for mentioned structures does not exceed 0.25, 0.3, 0.6 and 0.7 dB respectively. The power in these experiments is measured at the output of the waveguide, and all the value are compared to the first value in order to obtain relative change in the dB scale. To assure that these results are caused not by instability of the laser, measurements of laser output power were conducted and results are

presented in figure 5.5. It illustrates that fluctuations in the output power of the laser do not exceed 0.03 dB.

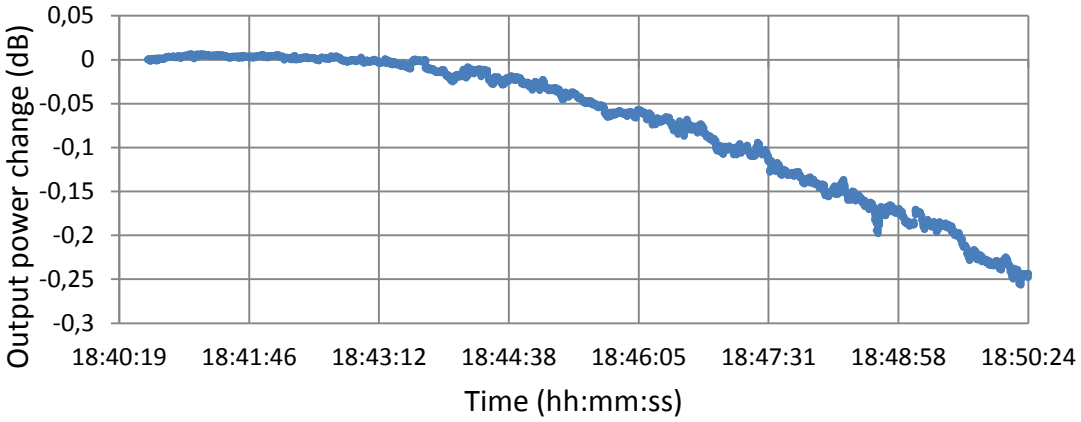

Figure 5.1: Output power change versus time for 1.5 µm wide straight waveguide

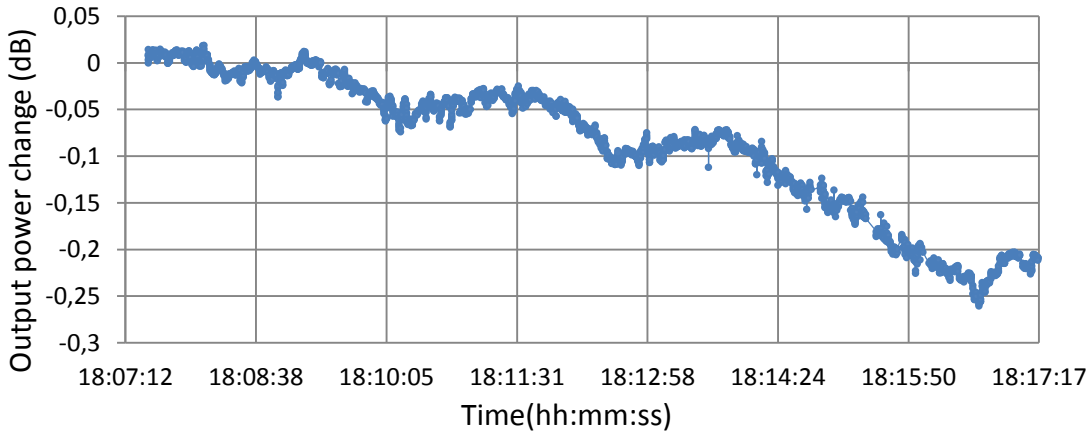

Figure 5.2: Output power change versus time for 3 µm wide straight waveguide

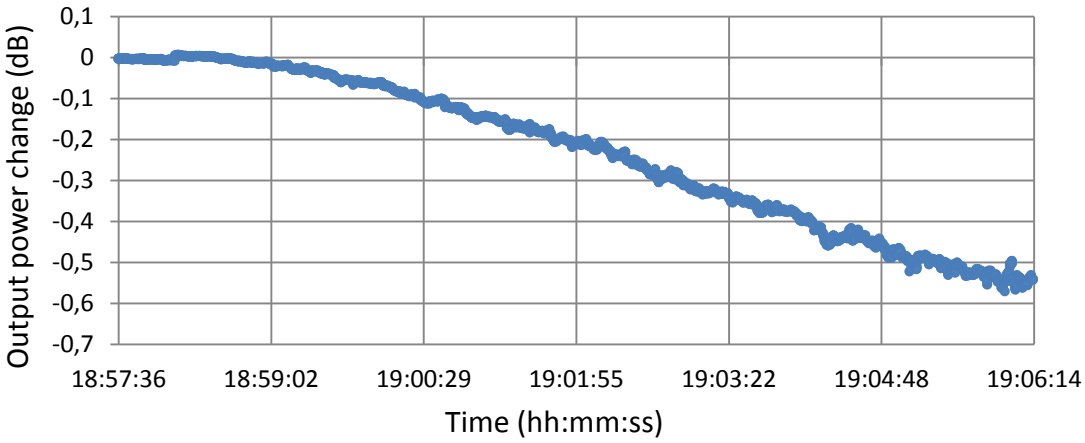

Figure 5.3: Output power change versus time for 10 µm wide straight waveguide

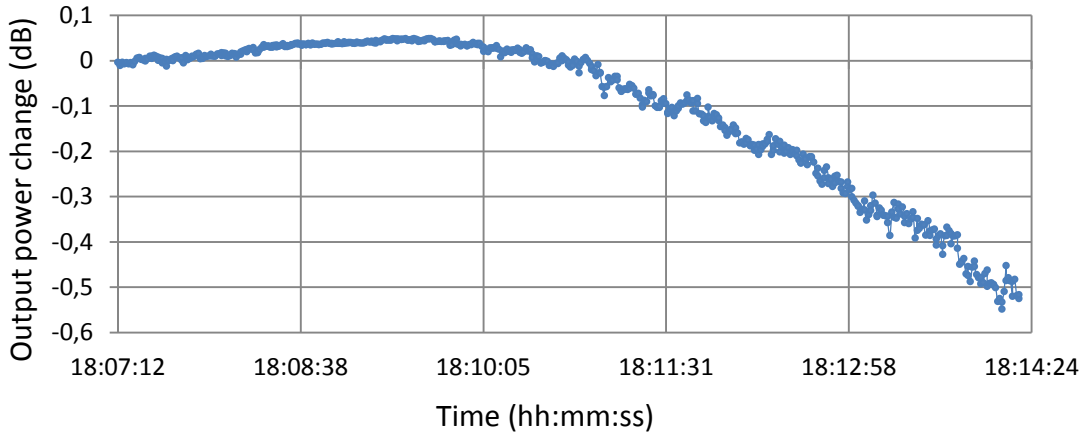

Figure 5.4: Output power change versus time for 3 µm wide balanced MZI

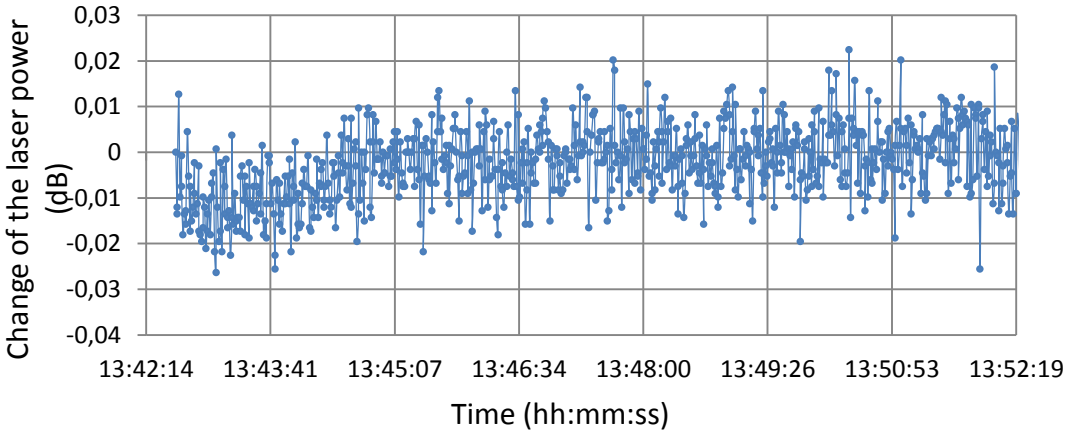

Figure 5.5: Change of the laser power output over time

From the results above it is clear that the power is not stable for specific temperature in the given time interval for all structures. The reason for the instability of the output power is mechanical drift of the stages that mount the chip, input and output objective lenses. Taking into consideration these instabilities of the power output, we proceed to study the output power stability of the whole system.

5.2 Output power measurement with change in temperature

In this section we conducted the power output measurements, changing at the same time the temperature of the chip. As it was mentioned in chapter 4, a Peltier element or a heating film was used to change the temperature.

5.2.1 Measurements with high input coupling and a Peltier element

This subsection is devoted to the first experiments performed with temperature variation. The procedure is the following: a chip is placed on the top of a Peltier element, which has a temperature sensor giving feedback to the temperature controller. Light is then coupled into a waveguide in such a way that the maximum output power is obtained. For the straight waveguide with a rib width 3 µm, the output power is approximately 3.5 mW. Coupling is carried out with a constant temperature; the initial value of the temperature is 25 °C. The first try is done by adjusting the temperature gradually by five degrees up to 30 °C. Power at the output of the waveguide is measured with power meter. Power variations from initial value versus time and temperature are shown in figures 5.6 and 5.7, respectively. Both charts illustrate that change in the power output is sharp and is 2 dB for 5 degrees temperature change. However, such a drastic change in power is not primarily due to changes in the waveguide caused by temperature, but rather due to thermal expansion of the stage holding the waveguide chip. Another reason is mechanical movement of a Peltier element. When a voltage is applied to the Peltier element, it expands.

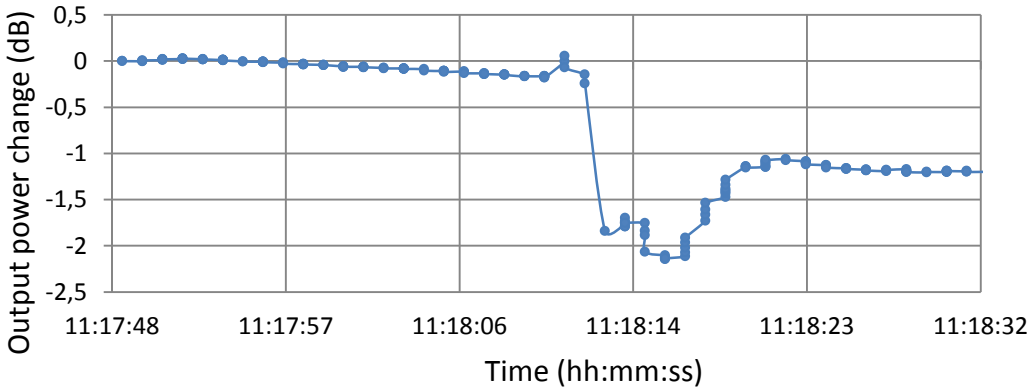

Figure 5.6: Power versus time for 3µm wide straight waveguide

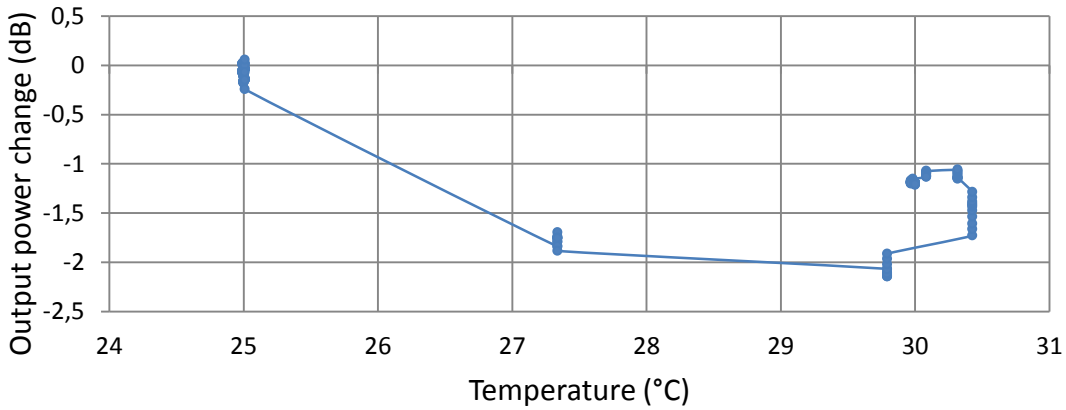

Figure 5.7: Power versus temperature for 3 µm wide straight waveguide

A method to attempt to avoid the influence caused by mechanical movement of the stage and Peltier element is described in the next chapter.

5.2.2 Measurements with reduced input coupling in combination with reference measurement

In order to reduce the influence of the chip movement, it was decided to pull the input objective lens a bit further away from the chip. Moving the lens back leads to defocusing of the coupling spot which becomes wider. The greater the spot, the easier it is to keep the waveguide input within its area. Power output obtained with this method is reduced and amounts to approximately ten percent of the maximum value gained with focused light beam. For instance, if the power output for a setup with focused beam is 3.5 mW, then objective lens is pulled back until the power is reduced to 0.3 – 0.4 mW. Unlike the previous experiment, the method described in chapter 4.2.3 is applied here, with reference power measurements carried out with the camera placed above the waveguide to sense the scattered light. It means that the results in figures 5.8 – 5.9 do not show the absolute value change, but the difference between power at the input and at the output.

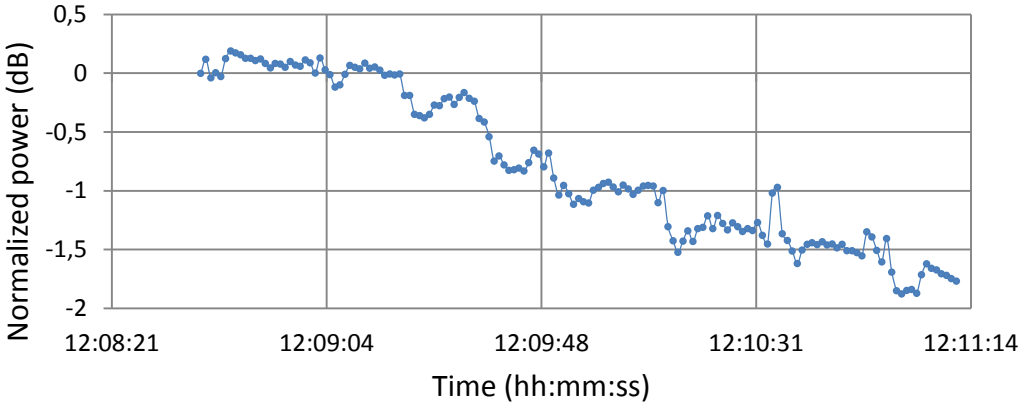

Figure 5.8: Normalized power change versus time for straight 2 μm wide waveguide and for 4 °C change in temperature

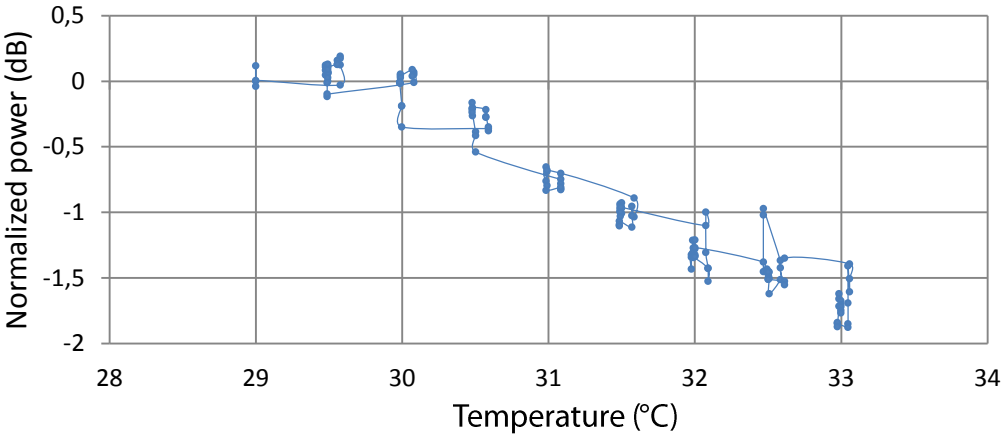

Figure 5.9: Normalized power change versus temperature for straight 2 μm wide waveguide and for 4 °C change in temperature

Results show that despite the widening of the light beam and normalization with a reference measurement, mechanical movement still affects the measurements. To eliminate this factor, the Peltier element was replaced by a heating film. One of the main advantages inherent to the Peltier element, however, is the ability to set and maintain the temperature constant, including temperatures below room temperature. On the contrary, a heating film can only be used for temperatures above ambient conditions and should

be regulated by a separate power source without feedback to a temperature controller.

5.2.3 Measurements performed with heating foil

The last group of experiments was conducted when the chip was placed on the top of a heating film instead of the Peltier element. The results are divided into three groups: for straight waveguide, normal Mach-Zehnder and unbalanced Mach-Zehnder interferometer. Each group includes data plotted in three graphs: the first plot shows the measurements used for normalization versus temperature. The second and the third plots illustrate variation of the output power normalized with the input power from the camera versus time and temperature, respectively.

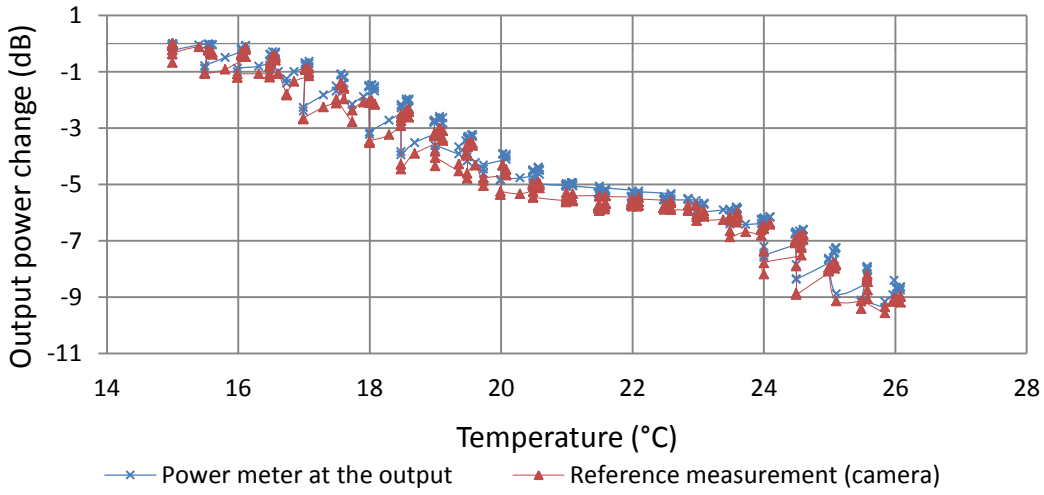

Figure 5.10: Power measured at the output and at the input for straight 2 μm wide waveguide and for 10 °C change in temperature

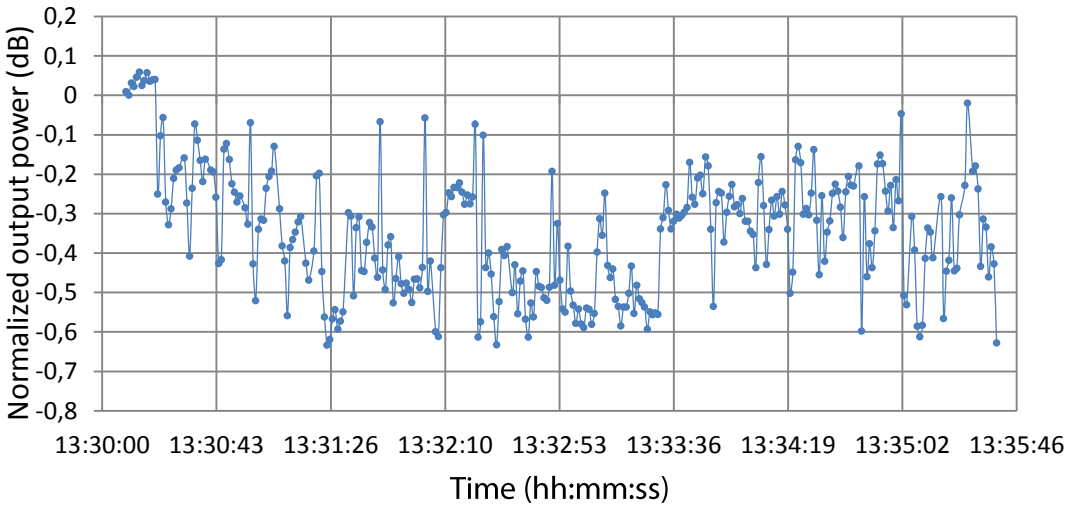

Figure 5.11: Normalized power change versus time for straight 2 μm wide waveguide and for 10 °C change in temperature

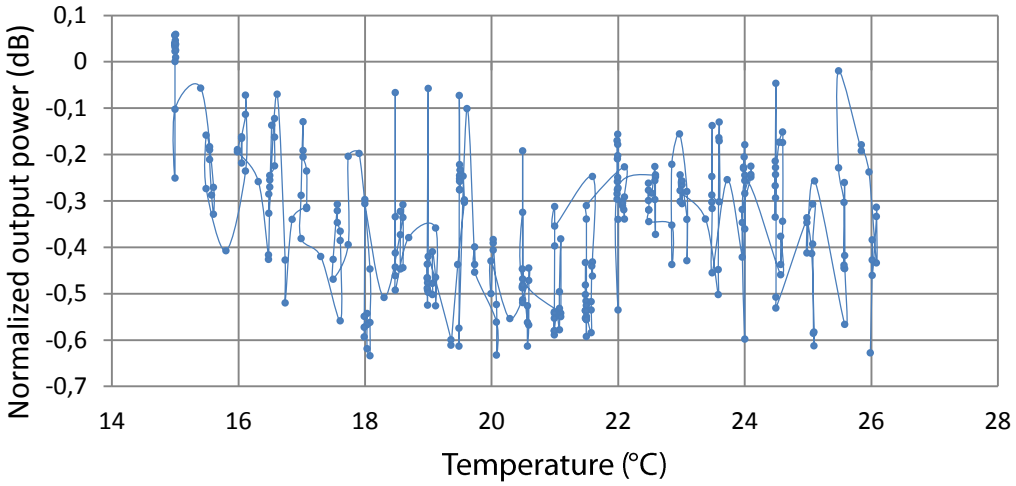

Figure 5.12: Normalized power change versus temperature for straight 2 μm wide waveguide and for 10 °C change in temperature

As it follows from figures 5.11 – 5.12, the normalized power variation for a straight waveguide is within 0.5 dB for 10 °C change in temperature, whereas without normalization it changes 9 dB (figure 5.10).

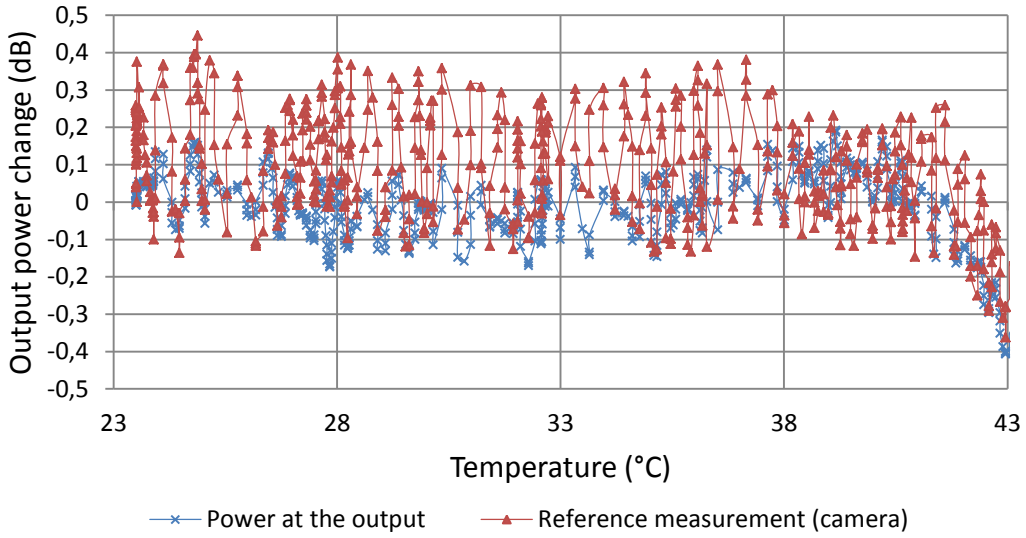

Figure 5.13: Power measured at the output and at the input for balanced 2 μm wide MZI and for 20 °C change in temperature

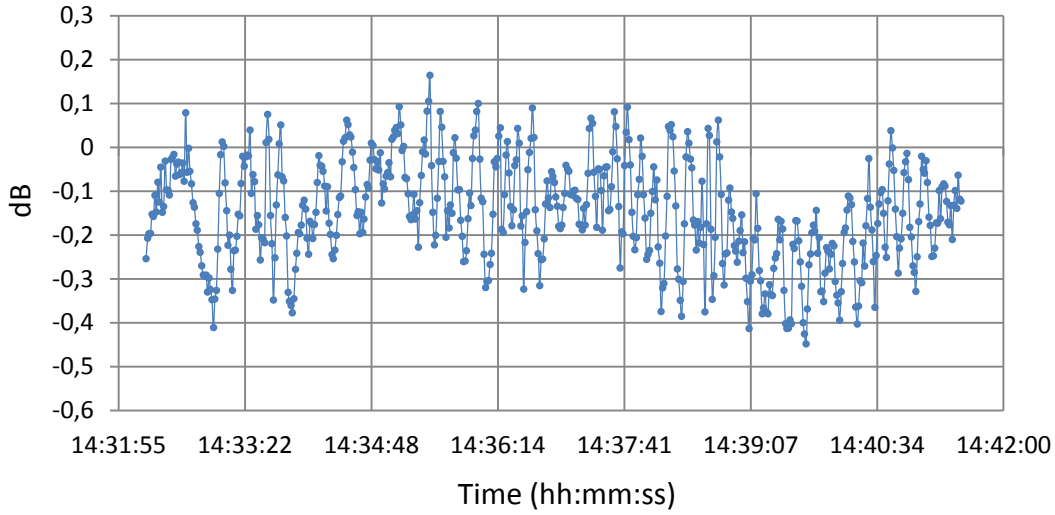

Figure 5.14: Normalized power change versus time for balanced 2 μm wide MZI and for 20 °C change in temperature

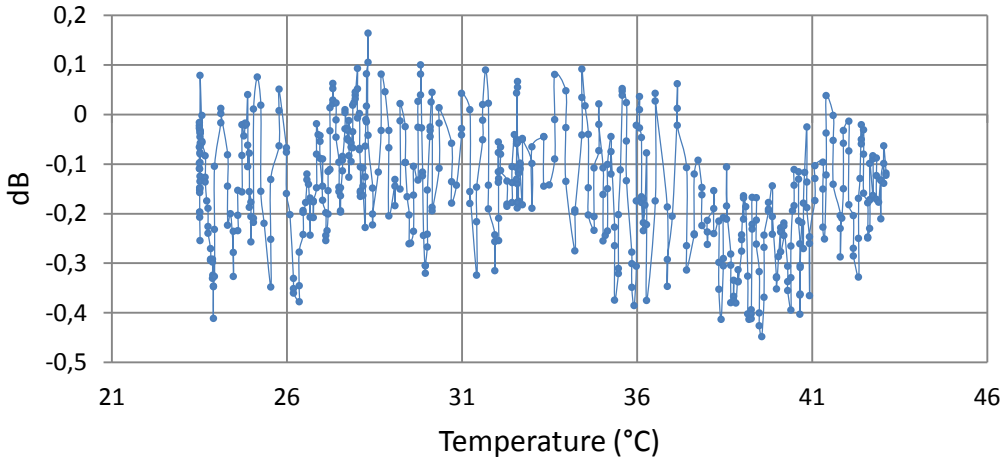

Figure 5.15: Normalized power change versus temperature for balanced 2 μm wide MZI and for 20 °C change in temperature

The normalized power variation for a balanced 2 μm wide Mach-Zehnder interferometer waveguide is within 0.5 dB for 20 °C change in temperature, whereas without normalization it changes 0.9 dB.

The last group of results illustrates the data obtained for the unbalanced Mach-Zehnder interferometer waveguide.

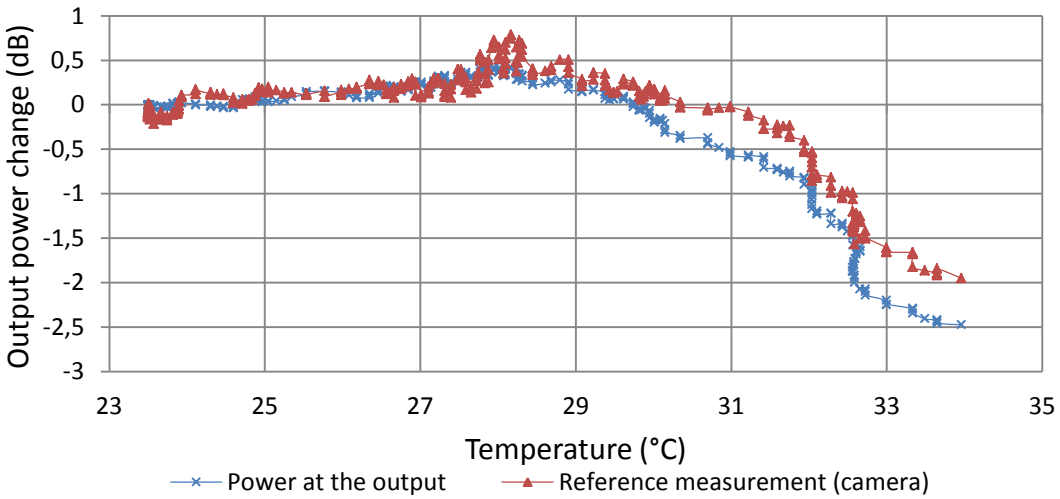

Figure 5.16: Power measured at the output and at the input for unbalanced 2 μm wide MZI for 10 °C change in temperature

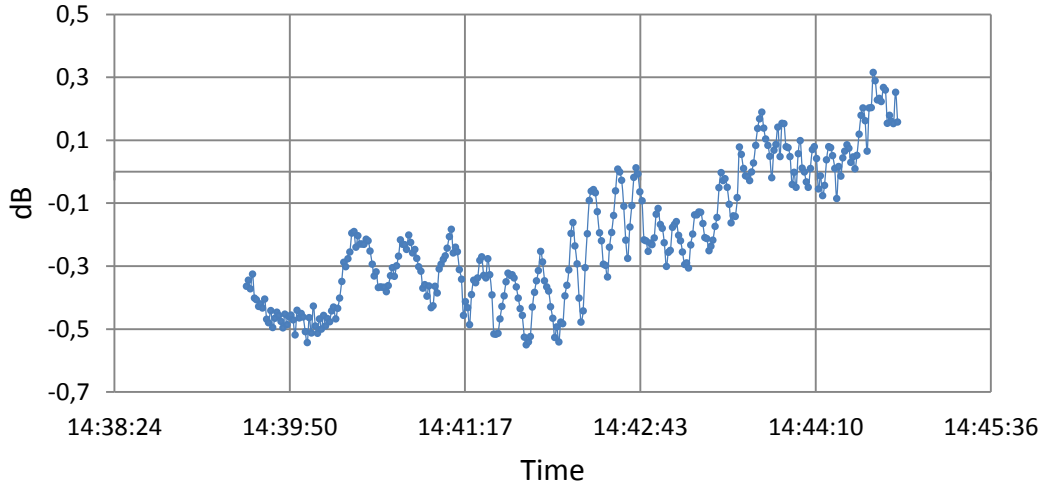

Figure 5.17: Normalized power change versus time for unbalanced 2 μm wide MZI and for 10 °C change in temperature

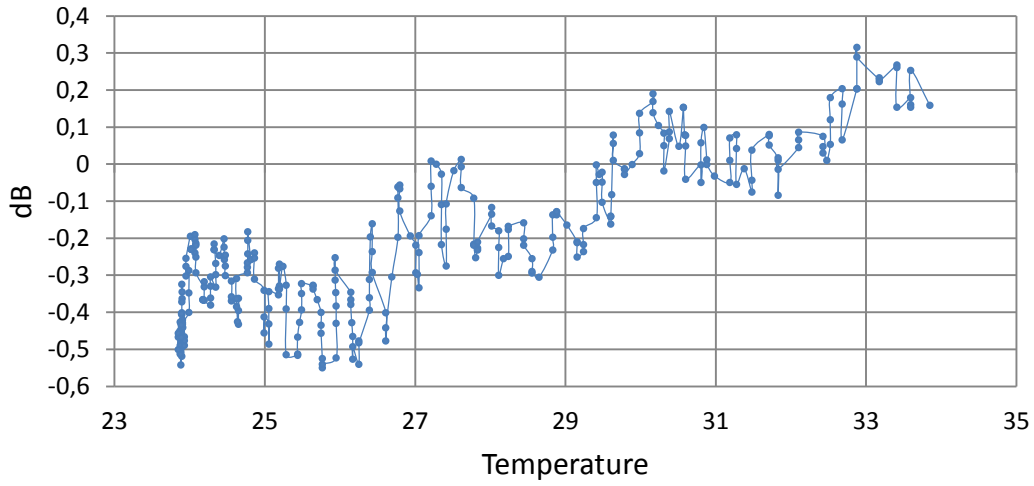

Figure 5.18: Normalized power change versus temperature for unbalanced 2 μm wide MZI for 10 °C change in temperature

The normalized power variation for the unbalanced 2 μm wide Mach-Zehnder interferometer waveguide does not exceed 0.9 dB for 10 °C change in temperature, whereas without normalization it changes 3.2 dB.

The measurement results show that the method implemented to reduce the influence of the chip movement works well. Moving the objective lens away from the waveguide chip, and applying reference power measurements carried out with the camera, we obtained the results indicating that for straight waveguide there is no significant dependence between the temperature change and the output power from the waveguide. For 10 °C change in temperature, the output power changes within 0.5 dB, and its plot is flat, with random variations along the horizontal axis.

The temperature increase for the experiments with balanced interferometer was 20°C to investigate a larger temperature range. Obtained results show that the output power changes within 0.5 dB again with only random variations, and correspond to theoretical analysis (chapter 2), which gave no temperature dependence.

Observed variation in the output power from unbalanced interferometer is 0.9 dB for 10 °C change in temperature. The intention was to conduct the experiments for a wider range of temperature. However, due to the instability in the setup it was not accomplished. Acquired results correspond well to the estimated variation of 1.1 dB in the output power. The plot of the power variation appears to be part of the cosine function, which the intensity should follow. Doing the experiments for a larger temperature range would confirm or refute this.

Chapter 6

Conclusion and further work

In this thesis the temperature effect on waveguide Mach-Zehnder interferometer (MZI) integrated on a waveguide chip have been experimentally studied. The Mach-Zehnder interferometer is the basis for a sensor that will be developed for methane sensing. The main application of this sensor is environmental monitoring of methane leakage. Temperature sensitivity of the device is important as it will be used in the environment where temperature difference can reach several tens of degrees, for instance in the air.

A mask representing the pattern of the chip layers was made during the work on this project. Also a LabView™ program was developed for logging the data acquired from a photo detector, which is connected to the temperature controller.

To investigate the temperature dependence, experiments were conducted for several waveguide structures: straight waveguides, balanced and unbalanced Mach-Zehnder interferometers. Balanced MZI has two arms of equal length, and unbalanced MZI has a 1 mm difference in length between the two arms. Input coupling has the major influence on the temperature sensitivity of the device. To reduce the impact from input coupling, objective lens was pulled away from the waveguide input, and a Peltier element was replaced by heating film. Significant improvement was achieved afterwards, when the reference measurements from the camera were implemented. The final results show good correspondence with estimates and demonstrate that

there is no significant dependence on the temperature change for the straight waveguide and the balanced Mach-Zehnder interferometer. The observed change in the output power for the unbalanced MZI is 0.9 dB for 10°C change in temperature, compared to an estimated variation of 1.1 dB. Further experimental work could confirm or refute the results of this study. The extension of the investigation could be made in a wider temperature range for different types of waveguide Mach-Zehnder interferometer, including unbalanced interferometers with larger length difference between the two arms.

Bibliography

[1] J. W. Steed, J. L. Atwood, *Supramolecular Chemistry*, second ed., 2009.

[2] V. M. N. Passaro, F. Dell'Olio, B. Casamassima, and F. De Leonardis, "Guided-wave optical biosensors", *Sensors 7*, pp. 508–536, 2007.

[3] S. E. Miller, "Integrated optics: An introduction", *The Bell Syst. Tech. J.*, vol. 48, p. 2059, Sept. 1969.

[4] D. Hondros and P. Debye, "Electromagnetic waves in dielectric wires", *Ann. Phys.*, vol. 32, pp. 465-476, 1910.

[5] E. Snitzer, "Cylindrical dielectric waveguide modes," *Journal of the Optical Society of America*, vol. 51, May 1961.

[6] E. A. J. Marcatili and R. A. Schmeltzer, "Hollow metallic and dielectric waveguides for long distance optical transmission and lasers", *The Bell Syst. Tech. J.*, vol. 43, July 1964.

[7] F. P. Kapron, D. B. Keck, and R. D. Maurer, "Radiation losses in glass optical waveguides", *Appl. Phys. Lett.*, vol. 17, pp.423 - 425, Nov. 1970.

[8] M. Lequime, "Fiber sensors for industrial applications," in *Proceedings of the 12th International Conference on Optical Fibre Sensors*, vol. 16 of OSA Technical Digest Series, pp. 66–71, OSA, Washington, DC, USA, 1997.

[9] R. Medlock, "Fibre optics in process-control", *Control Instrum*, vol. 21, no. 4, pp. 105–108, 1989.

[10] V. Demjanenko, R. A. Valtin, and R. A. Valtin, "A noninvasive diagnostic instrument for power circuit breakers", *IEEE Transactions on Power Delivery*, vol. 7, no. 2, pp. 656–663, 1992.

[11] K. Okamoto, "Recent progress of integrated optics planar lightwave circuits", *Opt. Quantum Electron*, vol. 31, pp. 107-129, 1999.

[12] P. K. Tien, "Integrated optics and new wave phenomena in optical waveguides", *Review of Modern Physics*, Vol. 49, No. 2, April 1977.

[13] R. G. Heideman, G. J. Veldhuis, E. W. H. Jager, P. V. Lambeck, "Fabrication and packaging of integrated chemo-optical sensors", *Sensors and Actuators B 35-36*, pp. 234-240, 1996.

[14] F. Rehouma, D. Persegol, and A. Kevorkian, "Optical waveguides for evanescent field sensing", *Appl. Phys. Lett. 65 (12)*, 1994.

[15] R.G. Hunsperger, *Integrated Optics, Theory and Technology*, 2009.

[16] F. Prieto, B. Sepulveda, A. Calle, A. Llobera, C. Domínguez, A. Abad, A. Montoya and L. M. Lechuga, An integrated optical interferometric nanodevice based on silicon technology for biosensor applications, *Nanotech. 14*, 2003.
[17] I. S. Duport, P. Benech, and R. Rimet, "New integrated-optics interferometer in planar technology", *Applied Optics*, 1994.

[18] K. Tiefenthaler and W. Lukosz, Sensitivity of grating couplers as integrated-optical chemical sensors, *JOSA B*, Vol. 6, Issue 2, pp. 209-220, 1989.

[19] H. Mukundan, A.S. Anderson, W. K. Grace, K. M. Grace, "Waveguide-Based Biosensors for Pathogen Detection", *Sensors*, 2009.

[20] C. L. Tien, T. W. Lin, "Thermal expansion coefficient and thermomechanical properties of SiN(x) thin films prepared by plasma-enhanced chemical vapor deposition", *Appl. Opt.*, vol.51, Issue 30, pp. 7229-7235, 2012.

[21] G. Ghosh, *Handbook of Thermo-Optic Coefficients of Optical Materials with Applications*, Academic Press, 1998.

[22] The GDS II Stream Format Manual, Jim R. Buchanan, 1996.

[23] Steven M. Rubin, "Computer Aids for VLSI Design", 1994.

[24] Donald L. Lee, *Electromagnetic principles of integrated optics*, Wiley,1986.

[25] B. Saleh and M.Teich, *Fundamentals of photonics*, Hoboken, New Jersey: John Wiley and Son, second ed., 2007.